

# Flood-pedestrian simulator for modelling human response dynamics during flood-induced evacuation: Hillsborough stadium case study

Mohammad Shirvani<sup>1</sup>, Georges Kesserwani<sup>1</sup>

<sup>1</sup>Department of Civil and Structural Engineering, University of Sheffield, Mappin St, Sheffield City Centre, Sheffield S1 3JD, UK

*Correspondence to:* Georges Kesserwani (g.kesserwani@sheffield.ac.uk)

**Abstract.** The flood-pedestrian simulator uses a parallel approach to couple a hydrodynamic model to a pedestrian model in a single agent-based modelling (ABM) framework on Graphics Processing Units (GPU), allowing dynamic exchange and processing of multiple agent information across the two models. The simulator is enhanced with more realistic human-body characteristics and in-model behavioural rules. The new features are implemented in the pedestrian model to factor in age- and gender-related walking speeds for the pedestrians in dry zones around the floodwater and to include a maximum excitement condition. It is also adapted to use age-related moving speeds for pedestrians inside the floodwater, with either a walking condition or a running condition. The walking and running conditions are applicable without and with an existing two-way interaction condition that considers the effects of pedestrian congestion on the floodwater spreading. A new autonomous change of direction condition is proposed to make pedestrian agents autonomous in way-finding decisions driven by their individual perceptions of the flood risk or the dominant choice made by the others. The relevance of the newly added characteristics and rules is demonstrated by applying the augmented simulator to reproduce a synthetic test case of a flood evacuation in a shopping centre, to then contrast its outcomes against the version of the simulator that does not consider age and gender in the agent characteristics. The enhanced simulator is demonstrated for a real-world case study of a mass evacuation from the Hillsborough football stadium, showing usefulness for flood emergency evacuation planning in outdoor spaces where destination choice and individual risk perception have great influence on the simulation outcomes.

## 1 Introduction

Flooding can disturb local communities such as in and around urban hubs, putting people at risk (Flood and coastal erosion risk management policy statement, 2020). In the lead-up to, and during, urban flooding, a number of underlying factors play a key role in determining flood risk to people, including human's physical, social and mental factors and flood-related factors, i.e. floodwater extent, depth and velocity (Ramsbottom et al. 2006; Milanese et al., 2015; Arrighi et al., 2017; Musolino et al., 2020; Moftakhari et al. 2018; Rufat et al., 2020; Hamilton et al., 2020; Bernardini et al., 2021). Understanding and quantifying

28 how the interplay between people- and flood-related factors affect the flood risk to people is a desired way forward (Aerts et  
29 al., 2018). In the context of flood risk management, there is a strategic need to develop methods and computational models to  
30 incorporate a combination of two or more of these factors (Priest, 2021). This is particularly required to make analysis of  
31 spatial and temporal changes in flood risk to people when they are directly exposed to floodwater, especially under immediate  
32 evacuation conditions (Bernardini et al., 2021). With the advances in computers, evacuation simulation models have been  
33 developed and calibrated to evaluate evacuation strategies according to the variability in the flood risk state of people. These  
34 models serve various purposes, such as finding the lowest-risk evacuation strategies by pinpointing bottlenecks, pathways and  
35 safe areas, estimating the time required to evacuate people and the time window for issuing an early evacuation warning  
36 (Aboelata and Bowloes, 2008; Lumbroso et al., 2011; Dawson et al., 2011; Mas et al., 2015; Liu and Lim, 2016; Bernardini et  
37 al., 2017; Zhu et al., 2019; Alonso Vicario et al., 2020).

38 Most of the existing evacuation models are built upon the soft agent-based modelling (ABM) paradigm for the  
39 representation of space-time distribution of a flooded population. ABM offers the flexibility needed to incorporate people-  
40 related factors to study their associated interactive and collective responses, either considered as moving individuals, groups  
41 of individuals in a vehicle, or household units (Zhuo and Han, 2020; Aerts, 2020). ABM-based tools are usually calibrated  
42 with evacuation behavioural rules to achieve more informed predictions for flood adaptation planning and extraction of  
43 decision-relevant indicators related to the dynamics of people's responses (Aerts et al., 2018; McClymont et al., 2019; Zhu et  
44 al., 2019). To account for flood-related factors, a two-dimensional hydrodynamic model is often used to feed information on  
45 the extent, depth and velocity magnitude of the floodwater as inputs into ABM-based evacuation models, from which the  
46 interactions across and between the people- and flood-related factors could be modelled (Dawson et al., 2011; Bernardini et  
47 al., 2017; Aerts, 2020). These interactions are organised to influence the evacuation behaviour of pedestrians, or agents, such  
48 as moving speed and stability states of people in and around the floodwater as they respond to an emergency warning while  
49 interacting with the features of an urban layout (Shirvani et al. 2020; Bernardini et al., 2021). Depending on the purpose of the  
50 model design and the targeted scale of application, the representation of the interactions across and between the people- and  
51 flood-related factors seem to require different levels of sophistication for the agent characterisation and evacuation behavioural  
52 rules.

53 For macroscale evacuation modelling, ABM-based models were developed to simulate immediate crowd evacuation  
54 from a city, focusing on moving groups of individuals or household units using cars within a city road network to analyse  
55 response time of aware and unaware people to the immediate evacuation warning (Dawson et al., 2011; Mas et al., 2015; Liu  
56 and Lim, 2016; Zhu et al., 2019; Alonso Vicario et al., 2020). These simulation models only consider vehicular emergency  
57 evacuation, which makes them not suited to simulate the interactive and the collective responses of moving individuals, or  
58 pedestrians, in and around small hubs ( $< 0.5 \text{ km} \times 0.5 \text{ km}$  in size), such as shopping centres or sports venues. For microscale  
59 evacuation modelling, where pedestrians need to be individually modelled, only a few ABM-based evacuation models were  
60 reported. One of these models is the Life Safety Model ([www.lifesafetymodel.net](http://www.lifesafetymodel.net)) developed by BC Hydro and HR  
61 Wallingford, which allows to analyse evacuation patterns of pedestrians along streetscapes and crossings (Lumbroso and Di

62 Mauro, 2008; Lumbroso and Davison, 2018). Another model is LifeSIM ([www.hec.usace.army.mil/software/hec-lifesim](http://www.hec.usace.army.mil/software/hec-lifesim)),  
63 developed by the US Army Corps of Engineers, which is capable of simulating individuals' responses to an emergency warning  
64 with the floodwater propagation, as they interact with the features of an urban layout, e.g. streetscapes and buildings (Aboelata  
65 and Bowles, 2008). These ABM-based evacuation simulation tools were developed to inform emergency plans for severe flood  
66 types, such as in the immediate aftermath of a dam-break or a tsunami wave (e.g. Lumbroso et al., 2021). The focus of these  
67 tools is mainly on estimating the loss of life, pinpointing bottlenecks and high-risk areas, and assessing how flood warnings of  
68 an impending flash flood could reduce the number of casualties and injuries. For this type of risk analysis, individuals'  
69 microscopic decisions and actions are considered insignificant in influencing the overall simulation outcomes due to the scale  
70 and speed of floodwater flow. However, for the most common flood types in urban areas, e.g. surface water due to extreme  
71 rainfall, less attention has been given to model the microscopic responses, down to the scale of the moving individuals, in and  
72 around flooded urban hubs (Ramsbottom et al. 2006). In this context, Bernardini et al. (2021) imported outputs of a flood  
73 model into a commercially available evacuation modelling tool, called MassMotion, to analyse flood risk differences in  
74 microscale and macroscale modelling with and without including pedestrians' microscopic evacuation behaviour. They  
75 concluded that incorporating pedestrians' microscopic evacuation behaviour in microscale modelling could significantly  
76 influence the spatial and temporal changes in flood risk to people, i.e. up to 15 % in absolute terms, when compared to  
77 macroscale modelling. Their findings also suggest the need to further incorporate non-homogeneous characteristics of people  
78 in a more flexible microscale modelling framework, which may result in additional differences to the analysis of flood risk to  
79 people.

80 One first effort in designing an ABM-based evacuation simulator capable of capturing microscopic responses at a  
81 small urban scale was taken by Bernardini et al. (2017). They developed FlooPEDS by incorporating the standard social force  
82 model for pedestrian dynamics (Helbing and Molnar, 1995), which was adapted to further model individuals' moving speed  
83 and stability states in floodwater. These states were implemented based on the experimental data and recommendations in  
84 Ishigaki et al. (2009), Chanson et al. (2014) and Matsuo et al. (2011), though individuals' way-finding decisions were solely  
85 influenced by behavioural rules of the social force model. The coupling with the hydrodynamic model was used to receive  
86 information on the changes in the floodwater conditions within the urban environment. However, FlooPEDS was reported to  
87 adopt a serial approach, by running one of the social force model and hydrodynamic model at a time, and a number of  
88 simplifications to alleviate runtime and dynamic memory costs, i.e. using uniform floodwater conditions on coarse  
89 subdomains, limiting the number of pedestrians up to 300 with uniform characteristics and the simulation time to less than 600  
90 s (Bernardini et al., 2017). Given its serial approach to the coupling, FlooPEDS is not ideally suited to incorporate the dynamic  
91 feedback from the moving pedestrians onto the floodwater flow. Shirvani et al. (2021) developed a flood-pedestrian simulator  
92 by taking a parallel approach to achieve the dynamic coupling between the hydrodynamic model and the social force model,  
93 both being ABM-based and running from a single ABM framework, Flexible Large-scale Agent-based Modelling Environment  
94 for the GPU (FLAMEGPU). The flood-pedestrian simulator on the FLAMEGPU framework benefits from the computational  
95 speed-up and high dynamic memory capacity of the Graphics Processing Unit (GPU). The latter property allows it to employ

96 as fine resolution and as large population size as needed with the hydrodynamic and pedestrian models, respectively (within  
97 the capacity of available GPU memory). This simulator is therefore supported with a two-way interaction condition to  
98 dynamically exchange agent information as they get updated across both the social force model and the hydrodynamic model.  
99 The two-way interaction condition allows to capture both the response of moving pedestrians to the floodwater and the back  
100 interaction of pedestrians' presence on the floodwater flow. Enabling the two-way interaction condition was found to  
101 significantly affect the model outcomes in and around congested areas: predict reduced flood risk for the pedestrians in **low-**  
102 **to-medium** risk areas and increased risk for those around high risk areas (Shirvani et al., 2021). In Shirvani et al. (2020), the  
103 social force model of the same simulator was further augmented with empirical datasets and experimentally derived formulas  
104 to incorporate non-uniform body characteristics and more variable moving speed and stability states of pedestrian agents in  
105 floodwater. The simulator was found to predict significantly prolonged evacuation times and higher number of at-risk  
106 pedestrians in low to medium risk areas in line with an increased sophistication in the pedestrian agent characteristics and  
107 behavioural rules (Shirvani et al., 2020), even without enabling the two-way interaction condition. In the latter version of the  
108 simulator, pedestrian agents were initialised to store body height and mass information, which were **key** human body factors  
109 considered to influence the determination of their stability states in the floodwater; and, were assigned variable moving speeds  
110 that are solely based on the mechanics of the floodwater. Also, the latter version of the simulator **was only applied to a synthetic**  
111 **test case and it was limited to a simplified way-finding decision rule for directing pedestrian agents to one fixed emergency**  
112 **exit destination (specified in advance). This means that the influence of the interplay between the two-way interaction condition**  
113 **and the pedestrian agent characteristics and rules on the simulation outcomes remained unexplored for real-world scenarios.**

114 This paper presents new developments in the flood-pedestrian simulator for incorporating a higher level of  
115 heterogeneity in pedestrian agent characterisation and more realistic behavioural rules than its previous version. The simulator  
116 is now augmented for real-world applications with new capabilities to account for:

- 117 • age, gender, body height and mass distribution of a subject population;
- 118 • age- and gender-related variable moving speeds of individuals in both dry and flooded zones based on real-world  
119 datasets and experimental information; and
- 120 • autonomous decision making of individuals in choosing one of multiple emergency exit destinations influenced by  
121 their personal perception of the risk from the floodwater or by the most popular destination selected by others.

122 These new developments are evaluated by analysing the associated changes induced in the simulated outcomes, by first  
123 contrasting them against the outcomes of the previous version of the simulator for a synthetic case study of a during-flood  
124 evacuation in a shopping centre; then, through a new real-world case study of a mass evacuation from the Hillsborough football  
125 stadium in response to a flood emergency replicating the conditions of November 2019 Sheffield floods.

126 This study is one step forward to developing an evacuation simulation tool, which intertwines an enhanced level of  
127 heterogeneity in agent characterisation and experimentally formulated behavioural rules for temporal and spatial microscopic  
128 flood risk analysis at individuals' level. The datasets of the simulated case studies and a video supplement that visualises

simulations in real time are openly accessible (Shirvani and Kesserwani, 2021b, Shirvani, 2021), as well as the source code of the latest version of simulator on FLAMEGPU (Shirvani and Kesserwani, 2021a) including a detailed user guide.

## 2 Material and methods

### 2.1 Overview of the flood-pedestrian simulator

The flood-pedestrian simulator dynamically couples a hydrodynamic model to a pedestrian model within the same ABM framework, FLAMEGPU (Shirvani et al., 2020; Shirvani et al., 2021). The pedestrian model adopts a standard social force model that accounts for the dynamic interactions occurring between moving pedestrians in a built environment (Li et al., 2019; Jiang et al., 2020). The pedestrians are represented by continuous space agents, each of which autonomously move in space and over time. The movement pattern of each pedestrian agent is derived by forces for avoiding collisions with their neighbouring pedestrian agents and with the key features within the environment layout, such as boundaries of the walkable area, terrain blocks and solid walls. The environment layout encodes force vector fields providing navigation to key destinations. These fields are stored within a grid of fixed discrete agents, forming a navigation map (Karmakharm et al., 2010). The navigation map is necessary for pedestrians' way-finding decisions while they are directed to reach their key destinations.

The hydrodynamic model is formulated based on a non-sequential implementation of a finite volume solver of the depth-averaged shallow water equations on a two-dimensional grid on FLAMEGPU, which was validated previously in Shirvani et al. (2021). The hydrodynamic model was applied on another fixed grid of discrete agents, flood agents, which is coincident with the grid of navigation agents. A flood agent stores information of the terrain properties in terms of height ( $z$ ) and Manning's roughness parameter ( $n_M$ ); and the state of floodwater variables in terms of depth ( $h$ ) and velocity components ( $u$  and  $v$ ). The state of floodwater variables is updated over time at each simulation iteration using the hydrodynamic model that operates for all the flood agents at the same time. Each navigation agent is set to store the updated state of floodwater variables from the coincident flood agent and subsequently provide this information to the pedestrian agent(s) at their location. The recipient pedestrian agents use the flood information to change their states based on a self-evaluative assessment of two criteria: Hazard Rating (HR) quantity of floodwater and human-body stability limits.

The HR quantity in pluvial or fluvial flooding with low probability of debris could be estimated as  $HR = (V + 0.5) \times h$  where  $V$  stands for the velocity magnitude estimated as  $V = \sqrt{u^2 + v^2}$  (Ramsbottom et al. 2006, Kvočka et al., 2016). Depending on the categorisation of the HR by the UK Environment Agency (EA), pedestrian agents are set to autonomously flag themselves with one of the four flood risk states: 'low' ( $0.0 < HR < 0.75$ ), 'medium' ( $0.75 < HR < 1.5$ ), 'high' ( $1.5 < HR < 2.5$ ) and 'highest' ( $2.5 < HR < 20$ ). In a similar way, the pedestrian agents are assigned a stability state which is also indicative of their mobility or immobility inside the floodwater. The stability state of pedestrian agents is estimated based on two experimentally derived formulas reported in Xia et al. 2014. These formulas evaluate the incipient velocity limits ( $U_c$ ) for

toppling and/or sliding conditions of human subjects in the floodwater by weighing the body height and mass information of each pedestrian agent as well as the states of floodwater variables. Depending on the evaluated  $U_c$  and the magnitude of the floodwater velocity ( $V$ ), the pedestrian agents are assigned one of four stability states: ‘stable condition’ where they carry on moving, or otherwise immobilised under ‘toppling-only condition’, ‘sliding-only condition’ or ‘toppling-and-sliding condition’ (see Shirvani et al. 2020 for more information).

The simulator is also supported with a functionality to enable a ‘two-way interaction condition’ to consider the effects that pedestrians’ congestion would have on altering the floodwater hydrodynamics, which can be significant as shown in Arrighi et al. (2017) and Shirvani et al. (2021). Hence, this condition incorporates any local and temporal changes in the state of the floodwater variables in a flood agent as a result of increased accumulation of pedestrian agents over the navigation agent at its coincident location. By enabling this functionality, the navigation agent is set to count the number of pedestrian agents ( $N_p$ ) that occupy its area at each time step. Then, the navigation agent uses  $N_p$  to alter local energy loss by locally updating  $n_M$  and passing it back to the coincident flood agent. The updated  $n_M$  is applied as  $n_M^{\text{updated}} = n_M + (N_p \times n_M)$ . The initial  $n_M$  parameter is set to be equal to  $0.01 \text{ s.m}^{-1/3}$ , representative of clear cement, and no more than 20 pedestrian agents are allowed to simultaneously occupy the area of a navigation agent, meaning that any local update in  $n_M$  cannot exceed  $0.2 \text{ s.m}^{-1/3}$ .

## 2.2 New characteristics and rules for pedestrian agents

### 2.2.1 Age, gender, and body mass characterisation

Each pedestrian agent is set to hold information of age, gender, and body mass at the time of its generation. To randomly assign an age, gender and body mass based on realistic distributions to each pedestrian, the UK national survey dataset (UK population by ethnicity, 2018) was used. As shown in Fig. 1, each pedestrian agent can have an age randomly selected from a range between 10 and 79 years old, and with a probability to keep the percentage of distribution of seven age groups. The excluded age groups, younger than 10 and older than 79 years old, make up 16 % of the UK population and represent children and elderly. To compensate for their exclusion, the percentage distribution of the other age groups was increased by around 2.3 %. Each pedestrian agent is also generated with a random ‘male’ or ‘female’ gender, each with equal chance of selection.

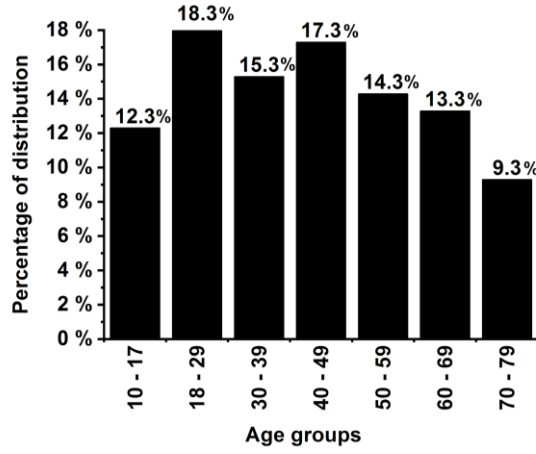


**Figure 1:** Age distribution assigned for the pedestrian agents in the flood-pedestrian simulator based on the UK's national survey (UK population by ethnicity, 2018).

Based on the age and gender of a pedestrian agent, its body mass, denoted by  $m_p$  (kg), is evaluated using the following formula (Disabled World, 2019):

$$m_p = l_p^2 BMI, \quad (1)$$

where  $l_p$  (m) stands for the body height of a pedestrian agent, which had already been incorporated within the previous version of the simulator (Shirvani et al., 2020). Here, the BMI (kg / m<sup>2</sup>) was randomly selected based on the ranges of age and gender listed in Table 1. For the age group between 10 and 17 years old, the BMI range was defined based on a standard for children (Prentice, 1998) and, based on samples of men and women who participated in the laboratory experiments reported in Bernardini et al. (2020) for the other age groups.

**Table 1:** Ranges of BMI used according to gender and age of individuals (details in Prentice (1998) and Bernardini et al. (2020)).

Age groups	Gender	BMI (kg / m <sup>2</sup> )
10 to 17	Both	Between 18.5 and 24.9
18 to 29 30 to 39 40 to 49 50 to 59 60 to 69 70 to 79	Male	Between 18.21 and 32.10
	Female	Between 16.01 and 32.03

### 2.2.2 Variable moving speeds

Each pedestrian agent is enabled to autonomously evaluate their variable moving speed according to their assigned age- and gender and the dynamic changes in the state of floodwater flow at their location. This was achieved by introducing two new sets of behavioural rules for all the pedestrian agents, governing the motion of the pedestrian agent in dry zones (around the

199 floodwater) and in flooded zones (inside the floodwater), respectively. To enable a pedestrian agent to discern between dry  
 200 zone and flooded zone, it resorts to the state of the floodwater's depth accessible from the navigation agent at its specific  
 201 location and time.

202 A pedestrian agent that identifies a zero depth of floodwater is automatically flagged to be in a dry zone. These  
 203 pedestrian agents are set to operate based on a 'dry-zone' moving speed rule under a walking condition. This rule assigns a  
 204 randomly selected walking speed to a pedestrian agent from a set of predefined ranges that are classified according to different  
 205 age and gender groups outlined in Table 2. The walking speed range of the 10 to 19 age group is defined according to the  
 206 human's average walking speed and is the same for both male and female (Mohler et al., 2007; Toor et al., 2001). For pedestrian  
 207 agents with 20 years of age and more, the ranges of their walking speed varies across different gender groups and are derived  
 208 from an empirically identified standard proposed by Bohannon and Andrews (2011). As people are expected to move faster  
 209 under evacuation conditions (Bernardini et al., 2020), pedestrian agents are applied an additional rule to increase their walking  
 210 speed based on the 'maximum excitement condition' identified in the experiments of Bernardini and Qualiarimi (2020). This  
 211 condition enables 'male' pedestrian agents to increase their walking speed by 60 % and 'female' agents to increase their  
 212 walking speed by 76 %. The experimental findings of Lee et al. (2019) also suggest a faster maximum excitement condition  
 213 for women, which may be associated with the fact that women have less tendency to be around floodwater compared to men  
 214 (Becker et al., 2015; Hamilton et al., 2020).

215  
 216 **Table 2:** Ranges of walking speeds for the pedestrian agents located in dry zones according to their age and gender (Toor et al., 2001; Mohler  
 217 et al., 2007; Bohannon and Andrews, 2011).

Age range (years)	Walking speed range (m/s)	
	Female	Male
10 to 19	1.39 to 1.47	1.39 to 1.47
20 to 29	1.270 to 1.447	1.239 to 1.443
30 to 39	1.316 to 1.550	1.193 to 1.482
40 to 49	1.353 to 1.514	1.339 to 1.411
50 to 59	1.379 to 1.488	1.222 to 1.405
60 to 69	1.266 to 1.412	1.183 to 1.300
70 to 79	1.210 to 1.322	1.072 to 1.192

218  
 219 A pedestrian agent that identifies a non-zero depth of floodwater is automatically flagged to be in a flooded zone.  
 220 These pedestrian agents are set to operate upon a 'flooded-zone' moving speed rule under either 'walking' or 'running'  
 221 conditions. With this rule, each pedestrian is assigned a moving speed that is evaluated by an empirical formula extracted from  
 222 the experiments in Bernardini et al. (2020). Denoting the moving speed of each individual by  $V_p$  (m/s), the formula reads

223 
$$V_p = a \cdot M^b, \tag{2}$$

where  $M$  is a function of **specific force per unit width** calculated by  $M = \frac{V^2 h}{g} + \frac{h^2}{g}$  with  $h$  and  $V$  being the depth and the velocity magnitude of floodwater respectively,  $g$  is the gravitational constant and  $a$  and  $b$  are age-related parameters defining each of the ‘walking’ and ‘running’ conditions, which are listed in Table 3.  $M$  is estimated at the navigation agent, where the pedestrian agent is present, from copies of  $h$  and  $V$  obtained from the flood agent at the coincident location. The validity of Eq. (2) is limited to subjects under the age of 68 and only applicable to floodwater depths between 0.2 m to 0.7 m (Bernardini et al., 2020). In reality, floodwater depth can be outside these limits and it may happen that an elderly beyond 68 years of age is present in a flooded area. Therefore, extra rules were applied to extend the variety of moving speed of pedestrian agents in flooded zones beyond the aforementioned age and floodwater depth limits for Eq. (2):

- the moving speed of pedestrian agents with an age greater than 68 is evaluated by decreasing  $V_p$  of the 61 to 68 age group by 1.6 % per year, following the experimental findings of Dobbs et al. (1993),
- pedestrian agents encountering a depth of floodwater shallower than 0.2 m are set to maintain dry-zone walking speed rule as they are not expected to experience significant interference from the floodwater on their walking speed (Lee et al., 2019), and
- pedestrian agents encountering floodwater greater than 0.7 m are given a moving speed informed by the stability limits reported in the UK’s Flood Risks to People method (Ramsbottom et al. 2006). Namely, these pedestrian agents are only set to have a moving speed when velocity magnitude  $V$  is less than 1.5 m/s, or otherwise, they remain immobile.

**Table 3:** The values of age-related parameters,  $a$  and  $b$ , identified by Bernardini et al. (2020) for evaluation of the moving speed of each individual under ‘walking’ and ‘running’ conditions via Eq. (2).

Age ranges (years)	Walking		Running	
	$a$	$b$	$a$	$b$
5 to 12	0.82	0.18	0.41	-0.21
13 to 20	0.54	-0.07	0.81	-0.19
21 to 28	0.36	-0.13	0.48	-0.19
29 to 36	0.35	-0.19	0.53	-0.23
37 to 44	0.43	-0.13	0.62	-0.20
45 to 52	0.57	-0.03	0.61	-0.17
53 to 60	0.32	-0.17	0.62	-0.20
61 to 68	0.16	-0.43	0.61	-0.17

### 2.2.3 Autonomous change of direction condition

Each pedestrian agent is also featured with two extra rules to enable it to autonomously navigate into new pathways while moving within a flooded zone, where it encounters a non-zero floodwater depth from the navigation agent at its specific time and location. The first rule makes a pedestrian agent detect and choose another destination if the floodwater depth along its

way becomes higher than a threshold of a floodwater depth to body height. The choice for the threshold is case-dependent and exploring different thresholds may be necessary (Sect. 4.2.2) as an individual's flood risk perception is dependent on different factors, including past flooding experiences (Hamilton et al., 2020; Abebe et al., 2020). This affects the modelling of decisions, i.e. when and where people enter the floodwater or make a move into another destination (Becker et al., 2015; Netzel et al., 2021). Applying this rule enables the pedestrian agents to make decisions on which pathway to take within an environment layout where there is no specific emergency exit at time of evacuation. The second rule applies to those pedestrian agents which remain undecided about selecting a pathway after a period of time (user-selected, Sect. 4.2.2). Such pedestrian agents are then set to detect the most popular destination chosen by the pedestrian agents within its surroundings. This rule is applied on the basis that group decisions have significant influence on the path finding decision of an individual in and around the floodwater (Becker et al., 2015; Lin et al., 2020).

### 3 Evaluation of the newly added characteristics and rules

The new characteristics and rules for pedestrian agents in the present version of the simulator were evaluated with a focus to assess their relevance for the analysis of pedestrian evacuation dynamics during a flood emergency (Sect. 3.3). Direct validation of agent-based models is a grand challenge as such models are aimed to study non-observable scenarios, where there is uncertainties associated with the emergent nature of behaviours and where validation datasets of such type are not available (An et al., 2020; Zhuo and Han, 2020; Aerts 2020). One alternative approach is a component-wise validation (Bert et al., 2014). This approach was used at the development stage of the dynamically coupled hydrodynamic and pedestrian models within the simulator (Shirvani et al., 2021).

To validate the relevance of in-model behavioural rules, one suitable strategy is to Take A Previous Model and Add Something (TAPAS) (Polhill et al., 2010; Abebe et al. 2020). This strategy was previously applied by systematically increasing the level of sophistication of agent characteristics and rules, and running the simulator progressively to identify their relevance by analysing the respective changes to the simulation outcomes (Shirvani et al., 2020). The TAPAS approach is also applied here to evaluate the new characteristics and rules added to the present version of the simulator, by setting it up and running it for the same test case used in Shirvani et al. (2020), Sect. 3.1, for five different configuration modes that are summarised in Table 4.

273 **Table 4:** Configuration modes used to set up and run the simulator to evaluate the newly added characteristics and rules.

Modes	Pedestrian behavioural rules				
	Two-way interaction	Moving speed in dry zones		Moving speed in flooded zone (Eq. (2))	
		Walking condition	Maximum excitement condition	Walking condition	Running condition
Mode 0	Disabled	Constant	Disabled	Age independent	Not applicable
Mode 1	Disabled	Age- and gender-related (Table 2)	Enabled (Sect. 2.2.2)	Age-related	Not applicable
Mode 2	Enabled				
Mode 3	Disabled			Not applicable	Age-related
Mode 4	Enabled				

274

275 **3.1 Overview of the flood evacuation in a shopping centre test case**

276 This test case was explored with the previous version of the flood-pedestrian simulator (Shirvani et al., 2020, Shirvani et al.,  
277 2021). It is reconsidered to assess the relevance of the new characteristics and rules added to the pedestrian agents within the  
278 present version of the simulator.

279 The test case considers a  $332 \times 332 \text{ m}^2$  hypothetical shopping centre that includes stores along its west and east sides,  
280 corridors and seven entrance/exit doors to the open space area (Fig. 2). The total walkable area of the shopping centre, including  
281 the open area and the corridors, is equal to  $70,350.8 \text{ m}^2$ , and 1000 pedestrian agents are generated to randomly occupy this  
282 space before the floodwater starts to propagate. The floodwater propagation was assumed to breach from the southern side  
283 along a 100 m opening (Fig. 2). When the floodwater starts to propagate, no more pedestrian agents are generated and the  
284 remaining ones are set to autonomously move to the emergency exit located at the northern side (Fig. 2), which is the only  
285 door open during the evacuation process.

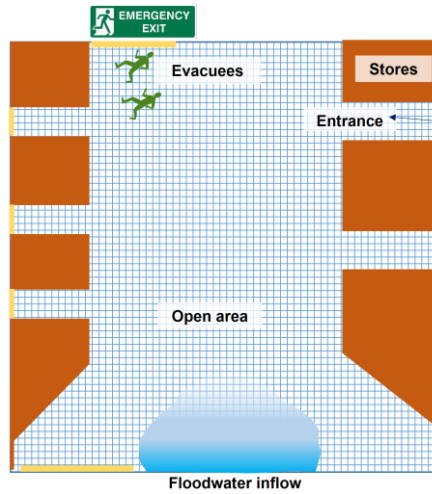


**Figure 2:** Sketch of the shopping centre: the meshed area in blue indicates the open area and corridors where pedestrians can walk to the entrance doors (coloured in yellow). Once the flood starts, evacuating pedestrians will go to the emergency exit (on the north side). The blocks in brown indicate terrain features assuming they are stores and the blue-shaded area in the southern part of the figure shows the location where the floodwater started to propagate.

The flooding inflow was generated based on an inflow hydrograph of a discharge,  $Q$  ( $\text{m}^3/\text{s}$ ) propagating over a duration of 7.5 min, and peaking to  $160 \text{ m}^3/\text{s}$  at 3.75 min (Fig. 3). The hydrograph was produced based on the Norwich inundation case study, and because it results in a range for the HR that is inclusive of all the ranges based on the EA categorisation, i.e.  $\text{HR} < 7$  (Shirvani et al., 2021). Deploying a hydrograph with shorter duration or a bigger peak would lead to significantly bigger HR, which is indicative of potential loss of life or injury where a person can take very limited actions to carry on moving to the emergency exit (hence is outside the scope of this study). When the floodwater starts to propagate over the walkable area, simulation time ( $t$ ) of 0 min, the pedestrian agents start the evacuation and the simulation terminates when all the pedestrian agents have evacuated the walkable area.

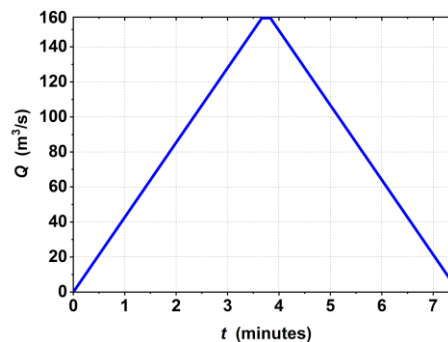


**Figure 3:** Inflow hydrograph that is used to generate the floodwater propagation from the southern side of the shopping centre.

### 3.2 Simulation runs

The simulator was executed at a resolution of  $2.59 \text{ m} \times 2.59 \text{ m}$  for each of the grids of navigation and flood agents. The time-step was taken to be the minimum between the adaptive time-step of the hydrodynamic model and the 1.0 s time-step of the pedestrian model (a visualisation of a simulation run can be found in the video supplement in Shirvani (2021)). In each run, the simulator is set to record the information stored in the flood agents and the pedestrian agents at each time-step. Recorded outputs from a simulation run include the positions of the pedestrian agents, their flood risk states (HR-related) and or their stability states (including toppling-only, toppling-and-sliding and sliding-only<sup>1</sup> conditions). As the motion of each pedestrian agent is governed by a stochastic (space-time) process, series of 10 and 20 simulation runs were conducted to average out a plausible outcome for each of the configuration Modes. The plausibility of the average outputs from both series of runs is evaluated, by estimating the margin of error (*MOE*) assuming confidence levels ranging between 90% and 99.9%. The following formula is used to evaluate the *MOE*:

$$MOE = Z_{score} \times \sqrt{\frac{\sigma^2}{n}}, \quad (3)$$

where,  $Z_{score}$  is the critical value, which is equal to 1.65, 1.96, 2.17, 2.58 and 3.29, for confidence levels of 90 %, 95 %, 97 %, 99 % and 99.9 %, respectively (Hazra, 2017);  $\sigma$  is the standard deviation from the sample of outputs of size  $n = \{10, 20\}$ ; and

$\sigma = \sqrt{\frac{\sum(x_i - \bar{x})^2}{n}}$ , with  $x_i$  representing the number of pedestrians with a particular HR-related flood risk or stability state extracted from the recorded outputs, and  $\bar{x}$  is the averaged value. Table 5 lists the maximum *MOE* evaluated for the different confidence levels, with respect to the average number of pedestrian agents under different HR-related flood risk and stability states for configuration Mode 0 to Mode 4.

**Table 5:** Maximum margin of error (*MOE*) for the average number of pedestrian agents with different HR-related flood risk or stability states that are extracted from the recorded outputs of all the configuration modes (Table 4) and across different confidence levels ranging from 90 % to 99.9%. Different ranges of the evaluated maximum *MOE* are highlighted with different colour shades: green, orange and red to indicate  $MOE \leq \pm 5$ ,  $6 \leq MOE \leq 9$  and  $MOE \geq 10$ , respectively.

Mode	HR-related flood risk and stability states	Maximum <i>MOE</i>									
		$n = 10$					$n = 20$				
		90 %	95 %	97 %	99 %	99.9 %	90 %	95 %	97 %	99 %	99.9 %
0	HR < 0.75	± 5	± 6	± 6	± 8	± 10	± 3	± 4	± 4	± 5	± 6
	0.75 < HR < 1.5	± 4	± 5	± 6	± 7	± 9	± 3	± 3	± 4	± 4	± 5
	1.5 < HR < 2.5	± 3	± 3	± 4	± 5	± 6	± 2	± 3	± 3	± 4	± 5
	HR > 2.5	± 1	± 1	± 1	± 2	± 2	± 1	± 1	± 1	± 1	± 1
	Toppling-only	± 5	± 6	± 7	± 8	± 10	± 4	± 4	± 5	± 6	± 8
	Toppling-and-sliding	± 4	± 5	± 5	± 6	± 8	± 3	± 4	± 4	± 5	± 9
1	HR < 0.75	± 6	± 7	± 8	± 9	± 12	± 4	± 4	± 5	± 6	± 7

<sup>1</sup> Although the sliding-only is implemented in the simulator, it is not expected to predict pedestrians under this stability state for the type of fluvial or pluvial floods investigated in this paper. This stability state would occur when pedestrians respond to raging and shallowly propagating floodwaters such as the case of a flash flood.

	0.75 < HR <1.5	± 6	± 7	± 8	± 10	± 12	± 4	± 4	± 5	± 6	± 7
	1.5 < HR <2.5	± 1	± 1	± 1	± 1	± 1	± 1	± 1	± 1	± 1	± 1
	HR > 2.5	± 0	± 0	± 0	± 0	± 1	± 0	± 0	± 0	± 0	± 0
	Toppling-only	± 6	± 8	± 8	± 10	± 13	± 4	± 4	± 5	± 6	± 7
	Toppling-and-sliding	± 5	± 6	± 7	± 8	± 10	± 3	± 4	± 5	± 5	± 7
2	HR < 0.75	± 6	± 7	± 7	± 9	± 11	± 4	± 5	± 5	± 6	± 8
	0.75 < HR <1.5	± 7	± 8	± 9	± 10	± 13	± 5	± 6	± 6	± 7	± 9
	1.5 < HR <2.5	± 1	± 1	± 1	± 2	± 2	± 1	± 1	± 1	± 1	± 1
	HR > 2.5	± 1	± 1	± 1	± 1	± 1	± 1	± 1	± 1	± 1	± 1
	Toppling-only	± 6	± 7	± 8	± 9	± 12	± 4	± 4	± 5	± 6	± 7
	Toppling-and-sliding	± 6	± 7	± 7	± 9	± 11	± 4	± 5	± 5	± 6	± 8
3	HR < 0.75	± 6	± 7	± 8	± 9	± 12	± 4	± 4	± 5	± 6	± 7
	0.75 < HR <1.5	± 6	± 7	± 8	± 9	± 12	± 4	± 5	± 5	± 6	± 8
	1.5 < HR <2.5	± 1	± 1	± 1	± 1	± 1	± 0	± 1	± 1	± 1	± 1
	HR > 2.5	± 0	± 0	± 0	± 0	± 0	± 0	± 0	± 0	± 0	± 0
	Toppling-only	± 6	± 7	± 8	± 9	± 12	± 4	± 5	± 5	± 6	± 8
	Toppling-and-sliding	± 6	± 7	± 8	± 9	± 12	± 4	± 4	± 5	± 6	± 7
4	HR < 0.75	± 5	± 6	± 7	± 9	± 11	± 4	± 4	± 5	± 6	± 7
	0.75 < HR <1.5	± 7	± 9	± 10	± 12	± 15	± 5	± 6	± 6	± 7	± 10
	1.5 < HR <2.5	± 1	± 1	± 1	± 1	± 2	± 1	± 1	± 1	± 1	± 1
	HR > 2.5	± 1	± 1	± 1	± 1	± 1	± 0	± 0	± 1	± 1	± 1
	Toppling-only	± 6	± 7	± 8	± 9	± 12	± 4	± 4	± 5	± 6	± 7
	Toppling-and-sliding	± 6	± 7	± 8	± 9	± 12	± 4	± 5	± 5	± 6	± 7

For  $n = 10$ , there is a considerable increase in the maximum *MOE* with Mode 1 to Mode 4 compared to Mode 0. This is particularly seen for the number of pedestrian agents in low and medium flood risk states ( $HR < 0.75$  and  $0.75 < HR < 1.5$ , respectively) and with toppling-only and toppling-and-sliding stability states. This suggests that the more sophisticated the pedestrian agent characteristics and rules, more discrepancies would appear in the simulator's outcomes. The maximum *MOE* identified suggests a deviation of around  $\pm 15$  from the averaged outcomes. However, when the sample size is increased to  $n = 20$ , the maximum margin of error does not exceed  $\pm 10$  for all the modes and confidence levels. Therefore, the simulation results analysed next are averaged out from a sample of 20 simulation runs, subject to  $\pm 10$  maximum *MOE* for a population of 1000 pedestrians in the flooded walkable area, which corresponds to a variance of 1 %.

### 3.3 Analysis of flood risks to people

Figure 4 shows the trends in the number of evacuating pedestrians with different HR-related flood risk states predicted by the simulator after 20 runs using all the configuration modes (Table 4). Figure 4a represents how the number of pedestrians with a low flood risk state ( $HR < 0.75$ ) change during 20 minutes of flood time. Figure 4a-left includes the trends predicted after enabling the walking condition for the age-related moving speeds (Mode 1) versus those predicted by further enabling the two-way interaction condition (Mode 2). In Mode 1, the trend is in good agreement with the baseline predictions (Mode 0, with non-age related moving speeds) at flooding times when there are less than 100 pedestrians in the walkable area with a low flood risk state, during 3.5 min to 7 min. A considerable difference among the predictions starts to appear when more than 150

341 pedestrians are present, around 2.5 min and 8.5 min. This difference seems to impact the overall trend, suggesting a 6 min  
342 longer duration with a higher number of pedestrians being predicted to be under this flood risk state, during 8 min to 18 min.  
343 In Mode 2, compared to Mode 1, the number of evacuating pedestrians is seen to reduce further at flooding times involving  
344 more than 150 pedestrians, around 2.5 min and 10 min. This is expected as crowding of pedestrians in low risk floodwaters  
345 would disperse the floodwater dynamics, which in turn help pedestrians evacuating ahead to pick up a faster moving speed  
346 (Shirvani et al., 2021). This does not seem to influence the collective moving speed of pedestrians, for example by generating  
347 additional congestions (as shown later in Fig. 6), as the overall trends with Mode 1 and Mode 2 are very close. Figure 4a-right  
348 contrasts the trends predicted after activating the running condition for the age-related moving speeds (Mode 3) to those  
349 predicted by also enabling the two-way interaction condition (Mode 4). In Mode 3 and Mode 4, the trends show a considerably  
350 faster moving speed of pedestrians (than with Mode 1 and Mode 2), significantly reducing the duration when pedestrians fall  
351 under a low risk state, suggesting outputs that are close to the baseline predictions (Mode 0). With Mode 3, discrepancies  
352 (compared with Mode 0) only occur between 2.5 and 3.5 min and after 8 min of flooding, when there are more than 150  
353 pedestrians moving under the running condition. In Mode 4, with further enabling the two-way interaction condition, the trends  
354 remain close to those predicted under Mode 3, except at 2.5 min flooding time that involves more than 200 pedestrians under  
355 a low flood risk state. This suggests that activating the two-way interaction condition with the running condition may only  
356 temporarily influence the pedestrians' collective moving speed, namely when more than 200 pedestrians are caught under a  
357 low flood risk state. Overall, there is a major difference in the collective moving speeds of pedestrians when age-related  
358 walking vs. running speeds are deployed, leading to prolonged vs. shortened evacuation times compared to the baseline  
359 predictions (Mode 0), respectively. Also, using the two-way interaction condition seems to be a sensible choice for simulating  
360 mass pedestrian evacuations in low risk floodwater.

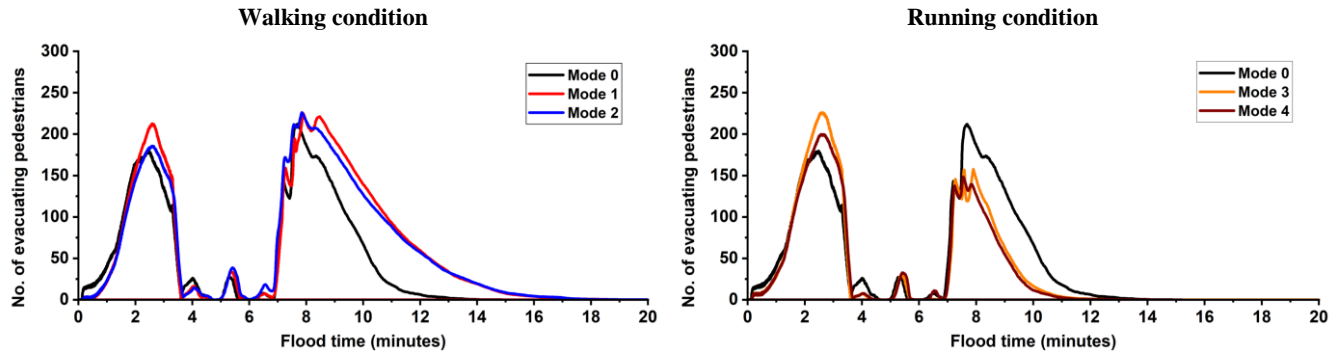
361 Figure 4b shows how the number of pedestrians with a medium flood risk state ( $0.75 < HR < 1.5$ ) change during 20  
362 minutes of flood time. With Mode 1 (Fig. 4b-left), compared to Mode 0, less number of pedestrians is predicted until 6 min,  
363 just before the number of pedestrians under this flood risk state reaches 300. This suggests that pedestrians could pick up faster  
364 moving speeds during the first 6 min of flooding, allowing them to escape medium risk floodwaters earlier. After 6 min, the  
365 trend with Mode 1 is fairly similar to the one with Mode 0, suggesting more influence of medium risk floodwaters on the  
366 collective moving speed of pedestrians irrespective of their age and gender. This difference is also marginal in the trends  
367 predicted by the simulator with Mode 2 that further activates the two-way interaction condition. However, like the trends seen  
368 for the low flood risk state (Fig. 4a-left), the pedestrians under a medium flood risk state exhibit a slightly faster moving speed  
369 when their number is over 300. Again, this could be related to more dispersions in floodwater dynamics due to large crowding,  
370 allowing the pedestrians located ahead to maintain faster moving speeds. By using instead the age-related running condition  
371 under Mode 3 (Fig. 4b-right), the trend observed is pretty similar to that with Mode 0, with slight differences appearing after  
372 6 min of flooding. Further enabling the two-way interaction condition (Mode 4) induces more reduction in the predicted  
373 number of pedestrians during the time of the flood when the crowding is at its peak, between 6 and 8 min (Fig. 4b-right). Also,  
374 the collective moving speed of pedestrians under either Mode 3 or Mode 4 is predicted to be similar to those under Mode 1

375 and Mode 2 for the pedestrians in a medium flood risk state. Hence, running the simulator with any of the configuration Mode  
376 1 to Mode 4 does not seem to make a major difference in the trends for the pedestrians with a medium flood risk state, all  
377 predicting considerably less numbers evacuating during early flood times before crowding occurs (compared to Mode 0).

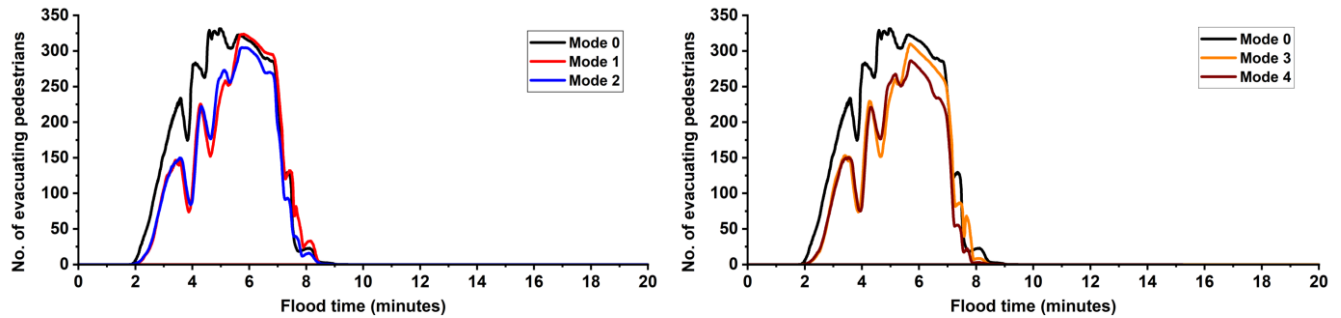
378 Figure 4c shows how the number of pedestrians with a high flood risk state ( $1.5 < HR < 2.5$ ) change during 20 minutes  
379 of flood time. For pedestrians with this flood risk category, running the simulator with any of the Mode 1 to Mode 4 leads to  
380 major differences in the trends compared to those predicted under Mode 0. With Mode 1 to Mode 4, only a handful of  
381 pedestrians are predicted to have a high flood risk state, during 3 min to 5 min of the flooding, in contrast to what the simulator's  
382 prediction with Mode 0 suggests: up to 140 pedestrians within a time window of 4 min. Hence, using the age-related moving  
383 speed, under either the walking condition or the running condition, seems to make a difference in the predicted trends in the  
384 number of pedestrians with a high flood risk state. The impact of the two-way interaction condition on the trends of such  
385 pedestrians can be detected by analysing the difference between the predictions made under Mode 1 vs. Mode 2, for the age-  
386 related walking condition (Fig. 4c-left), and between Mode 3 vs. Mode 4, for the age-related running condition (Fig. 4c-right).  
387 As can be seen, only a slightly higher number of pedestrians with a high flood risk state are predicted when the two-way  
388 interaction condition is also enabled, suggesting that it does not lead to major differences.

389 Figure 4d shows how the number of pedestrians with a highest flood risk state ( $2.5 < HR < 20$ ) change during 20  
390 minutes of flood time. In this case, with any of the Mode 1 to Mode 4, the simulator predicts only one or two pedestrians that  
391 could fall into this flood risk state around similar flood times predicted under Mode 0, which predicts a couple of more  
392 pedestrians under this flood risk state. This implies that using the age-related moving speeds can potentially predict less  
393 pedestrians that would be at the highest flood risk state. The trends predicted by the simulator using Mode 1 and Mode 3 are  
394 similar, indicating that using any of the running or walking conditions would lead to similar outcomes to inform on evacuating  
395 pedestrians with a highest flood risk state. These conditions combined with the two-way interaction condition (Mode 2 and  
396 Mode 4) leads to a slightly higher number of pedestrians with this flood risk state, as these pedestrians would be more affected  
397 by the local changes induced in the local floodwater dynamics from those pedestrians with a low risk state crowding ahead.  
398 Hence, either Mode 2 or Mode 4 seems to be a sensible configuration for the simulator to plan evacuation case studies involving  
399 more severe flooding scenarios.

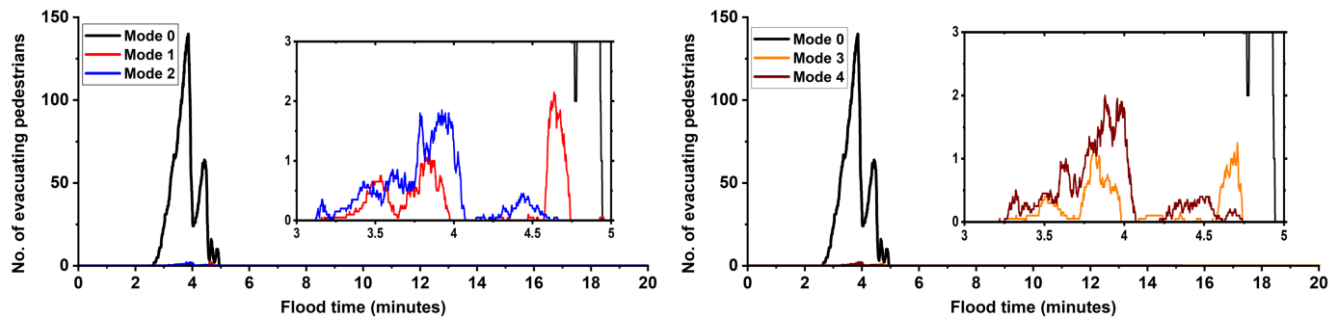
400  
401  
402



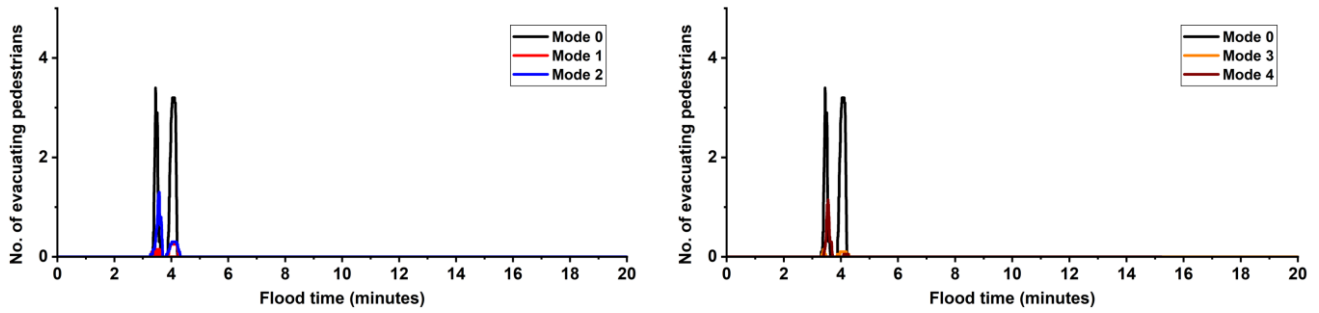
(a) Evacuating pedestrians with a low flood risk state ( $HR < 0.75$ )



(b) Evacuating pedestrians with a medium flood risk state ( $0.75 < HR < 1.5$ )



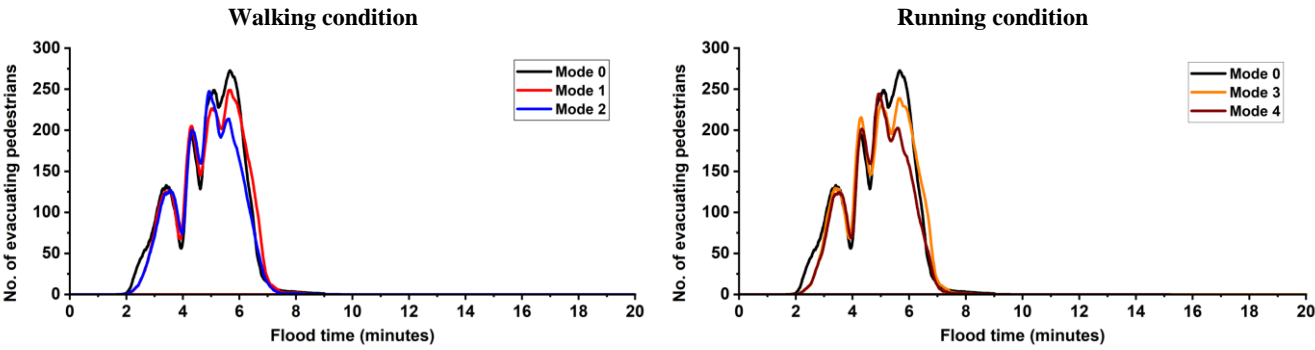
(c) Evacuating pedestrians with a high flood risk state ( $1.5 < HR < 2.5$ )



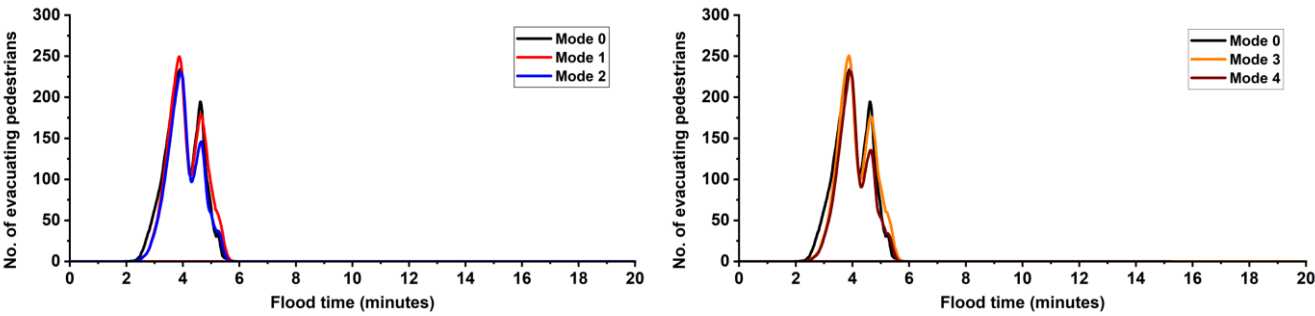
(d) Evacuating pedestrians with a highest flood risk state ( $2.5 < HR < 20$ )

**Figure 4:** Average number of evacuating pedestrians with different HR-related flood risk states predicted by the simulator after 20 runs under: Mode 0 (baseline outcomes from the previous version of the simulator, Shirvani et al., 2020); Mode 1 or Mode 2 (age-related walking condition for the moving speeds without or with the two-way interaction condition); and Mode 3 or Mode 4 (age-related running condition for the moving speeds without/with the two-way interaction condition). Analysis is presented in sub-figures (a)-(d), each considering a different flood risk state.

Figure 5 shows the trends in the number of evacuating pedestrians with different stability states averaged from the simulator predictions after 20 runs for all the configuration modes (Table 4). Pedestrians seem to be only under either toppling-only condition (Fig. 5a) or toppling-and-sliding condition (Fig. 5b), with no pedestrians spotted to be under a sliding-only condition. The trends predicted with the simulator under Mode 1 to Mode 4 lead to a similar timing, as the baseline prediction under Mode 0, when pedestrians potentially had toppling-only and toppling-and-sliding states: they show that these stability states could be detected during 2 min to 8 min, and during 2 min to 6 min, respectively. These flood times are found to contain a large number of pedestrians with low-to-medium risk states (Fig. 4a and b), suggesting that the majority of pedestrians within these flood risk states could be in toppling-only and toppling-and-sliding stability states. By also contrasting the outputs obtained from simulations under configuration Mode 1 and Mode 3, a very similar trend could be observed for the pedestrians with toppling-only (Fig. 5a) and toppling-and-sliding (Fig. 5b) stability states. This is also observed for the results with the simulator under Mode 2 and Mode 4, suggesting that age-related moving speeds lead to similar information on the stability states when the pedestrians have a low-to-medium flood risk state regardless of whether the two-way interaction condition is activated or not. Contrasting the trends without (Mode 1 and Mode 3) and with the two-way interaction condition (Mode 2 and Mode 4) shows notable reductions in the number of pedestrians at 6 min (Fig. 5a) and 4.6 min (Fig. 5b), during which large crowds ( $> 200$  pedestrians) were caught with medium risk states (see Fig. 4b). This observation suggests that running the simulator with age-related moving speeds with the two-way interaction condition (Mode 2 or Mode 4) is a sensible choice to study the stability state of large crowds in floodwater imposing low-to-medium risks to pedestrians. The evacuation patterns of pedestrians are analysed next through comparing their spatial distribution at 6 min of flood time across all the simulation modes, where the highest number of pedestrians are predicted to be at a medium flood risk state and the largest discrepancy in the number of pedestrians with a toppling-only condition is observed (see Fig. 4b and Fig. 5a).



(a) Evacuating pedestrians with a toppling-only condition



(b) Evacuating pedestrians with a toppling-and-sliding condition

431

432

433

434

435

436

**Figure 5:** Number of evacuating pedestrians with different stability states predicted by the simulator after averaging the results from 20 runs under: Mode 0 (baseline outcomes from the previous version of the simulator (Shirvani et al., 2020)); Mode 1 or Mode 2 (age-related walking condition for the moving speeds without or with the two-way interaction condition); and Mode 3 and Mode 4 (age-related running condition for the moving speeds without or with the two-way interaction condition). Sub-figures (a) and (b) include the stability states with a toppling-only condition and a toppling-and-sliding condition, respectively, when immobilised in floodwater.

437

438

439

440

441

442

443

444

445

446

447

Figure 6 compares the spatial distributions of the evacuating pedestrians over flood HR map at flood time 6 min, obtained from simulator runs under Mode 1 to Mode 4. In each of the sub-plots, the framed  $50 \times 50 \text{ m}^2$  before the emergency exit includes the number of pedestrians in that area, where the congestion of pedestrians is assessed for the different modes. With all the modes, the simulator predicted a dominance of medium risk floodwaters ( $0.75 < \text{HR} < 1.5$ ) over the walkable area, causing the majority of the pedestrians to fall into a toppling-only condition (purple dots) and a minority to have a stable condition (green dots) in front of the emergency exit and from the left side of the crowd. By contrasting the spatial distribution of pedestrians obtained from Mode 1 and Mode 2 (upper panels), there seems to be a considerable increase in the number of pedestrians with a stable condition when the two-way interaction condition is enabled with the walking condition (Mode 2). The same pattern is observed with Mode 3 and Mode 4 (lower panels), but this is accompanied by a shift in the position of pedestrians towards the front, as expected for the running condition. On the other hand, by contrasting the number of pedestrians in the small square obtained from Mode 1 and Mode 3 (left panels), it can be observed that enabling the running

condition results in a decrease in the congestion of pedestrians in front of the emergency exit. The opposite pattern is observed when enabling the two-way interaction condition in Mode 2 and Mode 4, showing an increase in the congestion of pedestrians under a running condition compared to the walking condition. Hence, using the two-way interaction condition with the simulator may be useful to more realistically evaluate bottlenecking impacts of an evacuation process.

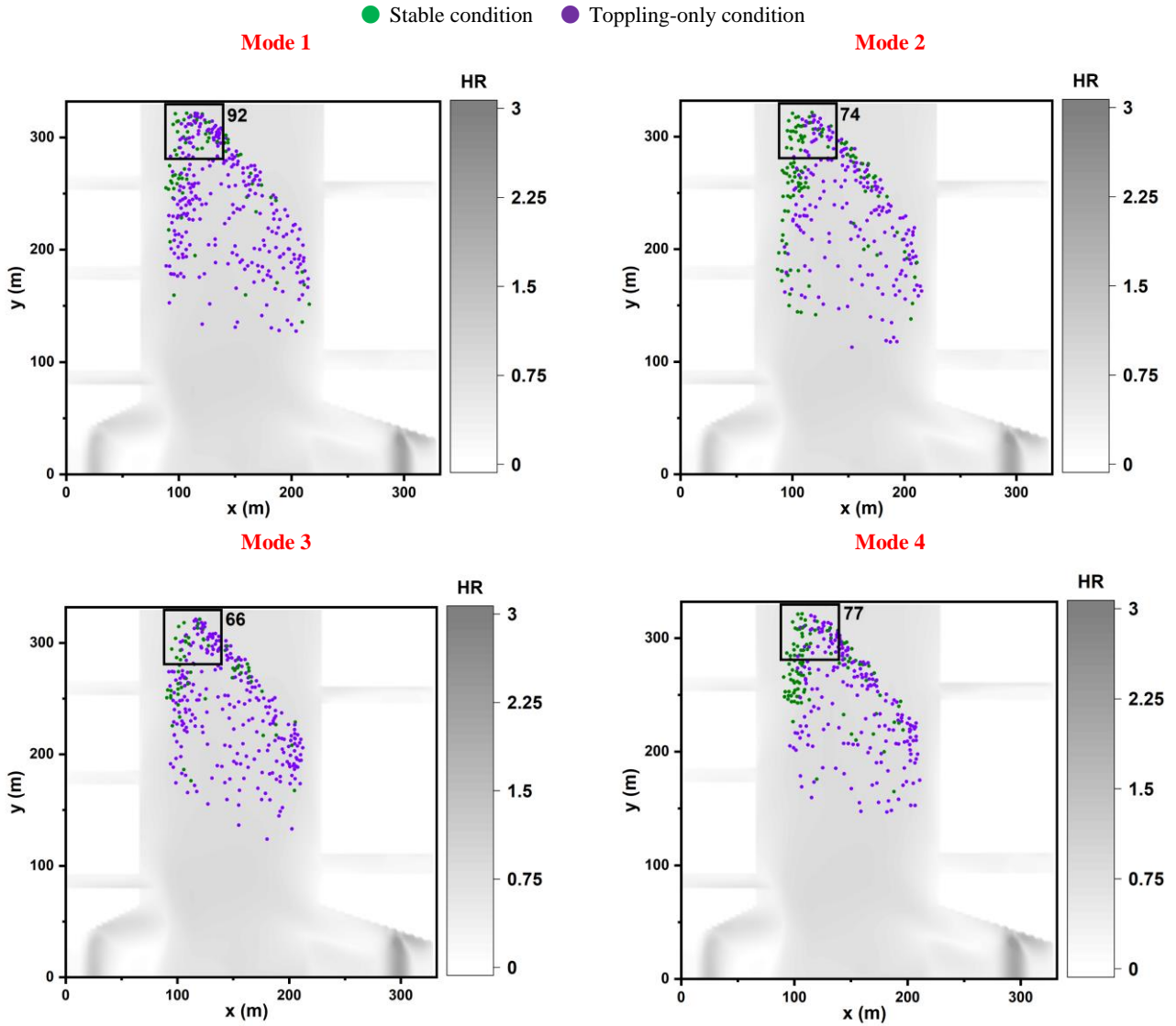


**Figure 6:** Spatial distribution of pedestrian agents, represented by coloured dots, predicted by the simulator under Mode 1 to Mode 4 at 6 min after flooding. The grey colour represents the floodwater extent based on the flood HR quantity and the square before the emergency exit represents an area of 50 × 50 m<sup>2</sup> with a number printed alongside it representing the number of pedestrians in that area.

In terms of total evacuation time for the 1,000 pedestrians, averaged results after 20 runs show that it takes 13.8 min with Mode 0, 18 min with Mode 1, 18.1 min with Mode 2, 12.5 min with Mode 3 and 12.3 min with Mode 4 to allow all the pedestrians to leave the walkable area. Contrasting the predicted times reinforces previous findings from Fig. 4: compared to Mode 0, the age-related walking speeds, either with or without the two-way interaction condition (Mode 1 and Mode 2, respectively), leads to slower evacuation speed predictions that become faster under the running condition.

Next, the simulator will be applied to analyse a scenario of mass evacuation of pedestrians during a pluvial flood leading to low-to-medium risk floodwaters in an urban neighbourhood. Supported by the analysis in Sect. 3.2 and Sect. 3.3, the simulator's configuration will be based on Mode 2 to produce conservative estimations of the evacuation time for planning and decision making.

## 4 Real-world case study

### 4.1 Background and scenario description

The case study consists of a site located outside of the main entrance of Hillsborough football stadium in Sheffield. The location of the site is framed with a dark red square in Fig. 7, including an area of 16,384 m<sup>2</sup> that is adjacent to the eastern side of the stadium, where the main entrances are located (yellow line, Fig. 7). The stadium entrances are opened to a T-junction that constitutes the walkable area whose boundaries are indicated by solid red lines. This area includes the main roads, main stadium's entrances, and pedestrian pathways to usual destinations to the south, east and north. These destinations, shown with the green lines in Fig. 7, are the most likely choices for a spectator leaving the stadium.



**Figure 7:** The study site (red square) including the walkable area (red area within the red square) where people normally use to go to their different destinations located in the south, east and north sides of the walkable area (green lines) after they leave the stadium from the main entrances (yellow line), © Google.

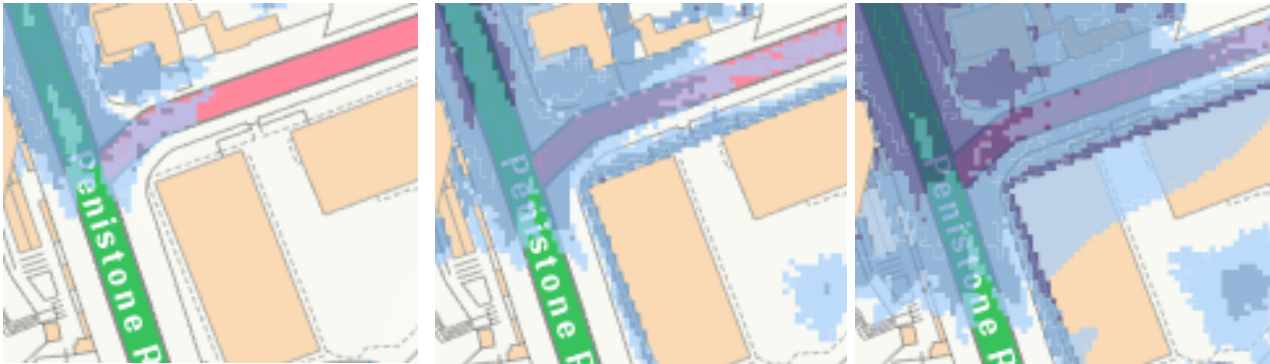
The stadium can accommodate up to 39,732 spectators with an average attendance rate of 24,000 per home football match in normal weather conditions (Sheffield Wednesday, available at: [www.footballwebpages.co.uk/sheffield-wednesday](http://www.footballwebpages.co.uk/sheffield-wednesday)). This site would therefore encompass a large number of spectators before or after a match, even in the aftermath of a flood as, for example, observed during the 2007 Summer floods (The Sheffield Guide by DeeJayOne, 2007; Environment Agency, 2007). The event suggests that rainfall runoff would cause floodwaters to spread from the east and north to accumulate in front of the main stadium's entrances, where it could submerge walking pathways, parking lots and the stadium pitch ("Bring on the sub", 2007). Worries of a similar event were expressed during the November 2019 floods driven by seven-day continuous rainfall of 63.8 mm over the city of Sheffield (Pugh, 2019), which led to cancelation of a football match as the flood defence protecting the stadium from River Don was about to be overtopped by the floodwater. The event, if happened during the football match, could put many in and around the stadium at a high risk.

This site, being both adjacent to River Don and located down the hills where rainwater runoff accumulates, has been flagged to be prone to future pluvial or fluvial flood types according to the EA's flood information service that is available online at <https://flood-warning-information.service.gov.uk/long-term-flood-risk>. This service provides flood maps for identifying long-term risks in parts of the UK towns based on a 'low', 'medium' and 'high' annual probability of occurrence. By entering the Hillsborough stadium postcode, S6 1SW, the flood maps showing the approximate ranges of the expected floodwater depth and velocity magnitude for the study site (Fig. 7) were obtained, as shown in the screenshots in Fig. 8. The floodwater depth map associated with a high annual probability (left panel, Fig. 8a) represents the least extreme scenario, where the range for the floodwater depth is likely to vary between 0.3 m and 0.9 m to potentially cover the northern branch of the walkable area with velocity magnitudes greater than 0.25 m/s. For a medium annual probability of occurrence (middle panel, Fig. 8a), the flooding extent could widen to potentially obstruct both northern and eastern branches with the range of floodwater depths reaching beyond 0.9 m and much wider extent for velocity magnitudes greater than 0.25 m/s mostly along the eastern branch (middle panel, Fig. 8b). For a low annual probability of occurrence (right panel, Fig. 8a), an even wider flood extent would be expected up to almost submerging the entire walkable area with dominance of deeper than 0.9 m floodwater depths along the northern branch and higher than 0.25 m/s velocities at the north, east and the sides of the southern branch. Even in the most optimistic flooding scenario, at least the northern branch near the stadium's entrance would be affected, where an evacuating spectator during a flood has to wade through floodwaters at a depth that is between 0.3 m and 0.9 m and velocities higher than 0.25 m/s. Therefore, investigating the dynamics of how people respond in a during-flood evacuation is of paramount importance for the selected study site.

‘High’ annual probability of occurrence: greater than 3.3 %

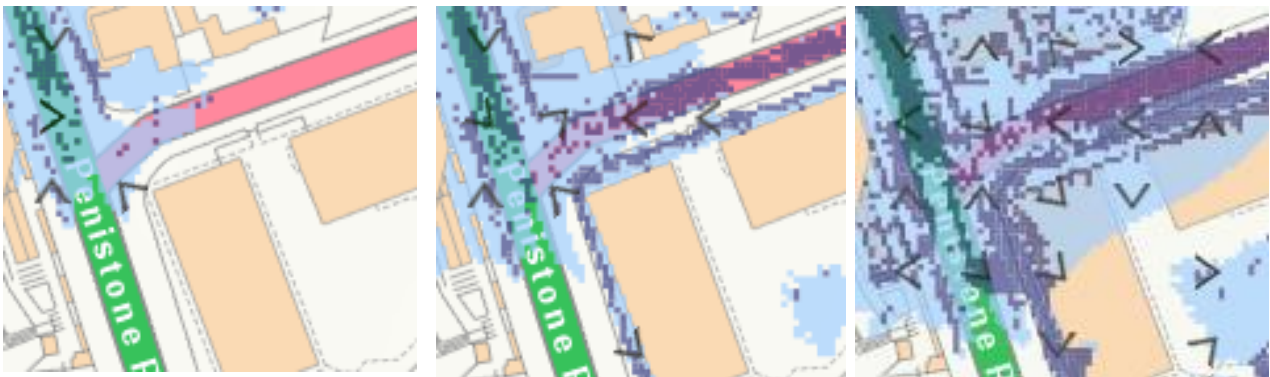
‘Medium’ annual probability of occurrence: 1 % and 3.3 %

‘Low’ annual probability of occurrence: 0.1 % to 1 %



●  $h$  greater than 0.9 m    ●  $h$  between 0.3 m and 0.9 m    ●  $h$  less than 0.3 m

(a)



●  $v$  greater than 0.25 m/s    ●  $v$  less than 0.25 m/s    < Direction of water flow

(b)

**Figure 8:** Screenshots of EA’s flood risk maps of the study site showing the extent of flooding from surface water with ‘low’, ‘medium’ and ‘high’ annual flooding probabilities featuring different floodwater ranges of: (a) depth and (b) velocity. These screenshots were retrieved from <https://flood-warning-information.service.gov.uk/long-term-flood-risk> (credit: © Crown and database rights under Open Government Licence v3.0).

To do so, it was assumed that the site in Fig. 7 is hit by a flood during a football match where the spectators are caught unaware of the rainfall accumulation around the stadium, similar to the event that could have happened in 2019. As discussed before, the floodwater is likely to accumulate from the north and east sides to move downhill towards the main entrance of the stadium. Once the floodwater has reached the stadium’s main entrances, an emergency evacuation alarm is issued, urging people to start evacuating immediately. The spectators are then put into queues inside the stadium to be evacuated towards the walkable area. The evacuating spectators gradually enter the walkable area where they get in direct contact with flooded areas

along their ways to any of the south, east or north destinations. In this scenario, a population of 4,080 spectators was assumed, which is lower than normal due to the severe weather condition and flood warnings issued prior to the event. This population is around 20 % of the spectators expected, and represents the relative number of people who would ignore the warnings and attend the match (Fielding et al., 2007).

For this case study, a dispatch measure was introduced to the simulator to release the evacuees into the walkable area during the flooding. The dispatch measure limits the influx rate to person-per-second per width unit to comply with guidance methods for controlling the density of large crowds outside the stadiums for safe evacuation (Minegishi and Takeichi, 2018; Still, 2019). For a gate that is around 4 m wide, four pedestrians per second are dispatched from the stadium to the walkable area. Using the simulator with this dispatch rate limits the overall number of pedestrians that would be present in the walkable area at a time. Therefore, running the simulator to analyse the evacuation of a larger number of spectators is expected to lead to similar risk trends based on pedestrians' different HR-related flood risk and stability states, which would only be prolonged over a larger evacuation time.

The flood-pedestrian simulator is applied to analyse how the number of pedestrians with different HR-related flood risk and stability states change under this scenario with a further focus on modelling their preference for the destination choice during the flood evacuation, by activating the 'autonomous change of direction' condition (Sect. 2.2.3).

## 4.2 Simulator configuration

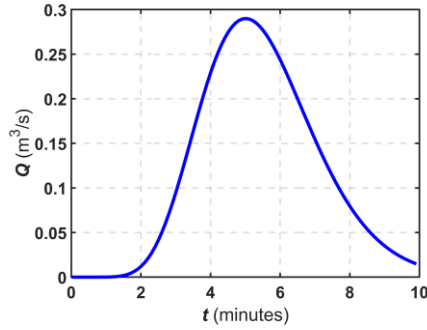
### 4.2.1 Hydrodynamic model set-up

The hydrodynamic model was set up to run on a grid of  $128 \times 128$  flood agents. The grid of flood agents (equally for the grid of navigation agents) was set to store the terrain features of the study site, loaded from a digital elevation model (DEM) at 1 m resolution, which is available online from the UK's Department for Environment Food & Rural Affairs (DEFRA) LiDAR Survey at: <https://environment.data.gov.uk>. To the best of the authors' knowledge, there is no record of any observed hydrograph sampled at a gauge point located in the selected study site. Therefore, the flooding flow was generated by formulating an inflow hydrograph based on the November 2019's rainfall volume (Fig. 9). The hydrograph was set to replicate a total runoff volume accumulation of 1,045.3 m<sup>3</sup> based on a 0.0638 m rainfall over the entire 16,384 m<sup>2</sup> site. This volume was estimated using the direct runoff method:  $rainfall\ volume\ (m^3) = rainfall\ height\ (m) \times area\ (m^2)$ . The hydrograph was generated as:

$$Q_t = Q_{initial} + (Q_{peak} - Q_{initial}) \left( \frac{t}{t_{peak}} \cdot \exp\left(\frac{1-t}{t_{peak}}\right) \right)^\beta, \quad (4)$$

where  $Q_t$  (m<sup>3</sup>/s) is the inflow discharge propagating along the north-east boundary intersecting the eastern branch;  $Q_{peak}$  (m<sup>3</sup>/s) = 0.29 is the peak discharge, that was calculated by distributing the runoff volume (1,045.3 m<sup>3</sup>) per second over an hour of flooding;  $Q_{initial}$  (m<sup>3</sup>/s) is the initial discharge, taken 0 m<sup>3</sup>/s;  $t$  (min) is the simulation time varying between 0 to 10 min;  $\beta =$

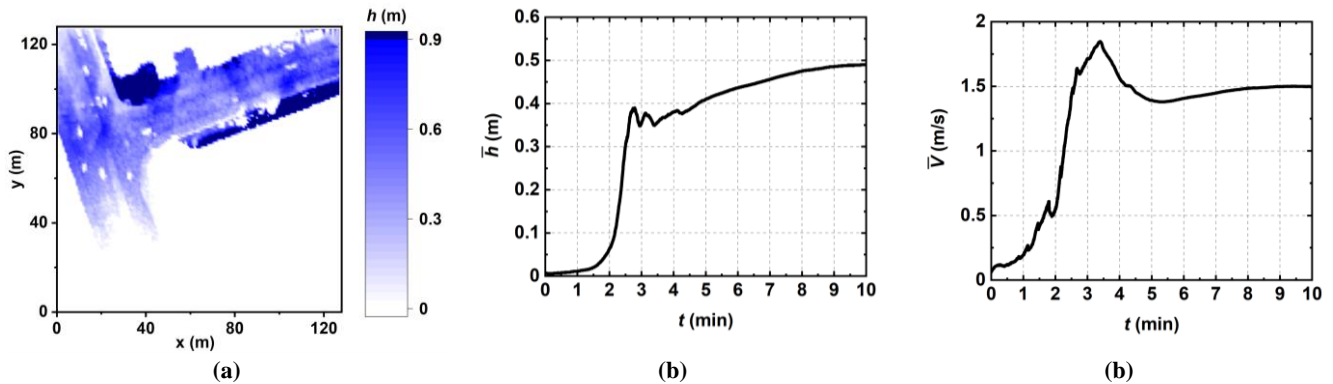
10 is a constant to soften the shape of the hydrograph and  $t_{peak}$  (min) = 5 is the time of peak discharge. This choice, for  $t_{peak}$ , considers the peak discharge has been reached halfway during the flooding to cause the propagating floodwater to reach to the main stadium's entrances by 10 min leading to triggering the evacuation alarm.



555

556 **Figure 9:** Inflow hydrograph produced by Eq. (4) used to generate the floodwater propagation occurring from the north-east side of the site.

557 To ensure that the resulting ranges of floodwater depth and velocity magnitude generated by the hydrograph in Fig.  
 558 9 fit the expected ranges of floodwater depth and velocity reported by the EA, a run was conducted without pedestrian  
 559 consideration. Fig. 10a shows the map of the predicted floodwater depth after 10 min of flooding, while Fig. 10b and Fig. 10c  
 560 includes the time series of the mean floodwater depth ( $\bar{h}$ ) and velocity magnitude ( $\bar{V}$ ) in the lead-up to 10 min, respectively.  
 561 From the floodwater depth map, it can be seen that the spatial distribution of floodwater depth varies between 0.3 m and 0.9  
 562 m inside the walkable area at the time when pedestrians start to evacuate. By this time, Fig. 10b and Fig. 10c suggest that the  
 563 mean floodwater depth is at its deepest level of 0.5 m and the velocity magnitude reduces to 1.5 m/s. Beside confirming that  
 564 the generated hydrograph leads to a realistic flood event in line with the EA's expectations, these results indicate that a  
 565 pedestrian evacuating into the floodwaters shown in Fig. 10a would be under a low-to-medium flood risk state with an HR  
 566 value estimated around 1 (can be extracted by the end of the time series in Fig. 10b and Fig. 10c).



567 **Figure 10:** Outputs of the simulator generated after and during 10 min of a single hydrodynamic run without pedestrian consideration plotted  
 568 in terms of: (a) floodwater depth map and temporal changes in the average floodwater in terms of (b) depth and (c) velocity.

#### 4.2.2 Pedestrian model set-up

The pedestrian model was also set up for a grid of  $128 \times 128$  navigation agents encoding the topographic features of the site into the navigation map as well as the boundaries, location of entrances and destinations about which the pedestrian agents receive information. The pedestrian model was set to gradually generate 4,080 pedestrian agents with a rate of 4 pedestrian agents per second starting at simulation time  $t = 0$  min. Once a pedestrian agent is generated, it is assigned a random (initial) destination between the south, east or north (Fig. 7) with an equal probability of selection.

As the case study consists of an outdoor urban environment with multiple destination choices, the pedestrian agents are set to dynamically alter their initially assigned destination by activating the ‘autonomous change of direction’ condition (Sect. 2.2.3). This condition allows pedestrian agents to auto-select new pathways after analysing the state of the floodwater variables received from the navigation agent at their current location. As explained in Sect. 2.2.3, this condition requires specifying a threshold of floodwater depth to body height beyond which a pedestrian agent considers shifting their walking direction and looking for a new destination within 100 seconds. After this period, if the pedestrian agent remains undecided, it is set to pick the destination selected by the majority of its neighbouring pedestrian agents, on the basis that it was influenced by the choice of others around (Sect. 2.2.3).

For the ‘autonomous change of direction’ condition, three thresholds of floodwater depth to the body height (Fig. 11) were selected, informed by the experiments in Dias et al. (2021). This was done to account for the uncertainty associated with individuals’ different risk perception. The ‘20 % threshold’ was defined to represent people with high-risk perception, such as those who previously experienced a critical flooding incident, and decide not to enter floodwater with a depth that is more than 20 % of their body height. This threshold is estimated based on the ratio of the dominant minimum value for the depth of floodwater that can occur over the walkable area (0.3 m) to the height of the shortest pedestrian agent available (1.4 m). With this threshold, the likelihood of the entire population to be in a condition to change their direction is ensured. The ‘40 % threshold’ was defined to represent people with low-risk perception, such as those who have not yet experienced a flood incident, and decide to enter a floodwater with a depth that is even more than 40 % of their body height. This threshold is estimated based on the ratio of the dominant maximum depth of floodwater (0.9 m) to the height of the tallest population of pedestrian agents available (2.1 m). This threshold enables the entire population to have the freedom to keep moving even within the deepest floodwater in the walkable area (0.9 m). The ‘30 % threshold’ accounts for an average-risk perception, such as those who previously experienced a minor to moderate flooding incident. Pedestrians with average-risk perception would decide to enter floodwater up to their knees, which constitutes 30 % of the human body height (Teichtahl et al., 2012).

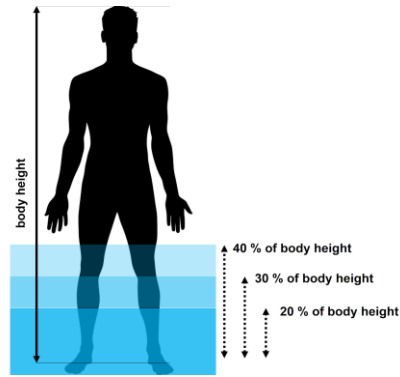


**Figure 11:** Thresholds of floodwater depth to body height that are specified for pedestrian agents to accommodate uncertainty associated with different risk perception of people in the real-world case study.

The characteristics of pedestrian agents were adapted to consider the age, gender and height distribution of football fans in the UK. Therefore, the randomised age distribution reported in Sect. 2.2.1 was increased by 5 %, 8 % and 4 % for the age groups of 30 to 39, 40 to 49, and 50 to 59 to replicate the higher attendance of these age groups to live sports events in England (Lange, 2020). Also, the randomised gender distribution was changed to 67 % males and 33 % females based on a survey on the gender distribution of football fans in the UK (Statista Research Department, 2016). In terms of body height, the pedestrian agents were based on the same UK body height distribution used previously (Shirvani et al., 2020).

#### 4.2.3 Simulation runs

A series of 20 simulation runs was performed under configuration Mode 2 for each of the 20 %, 30 % and 40 % threshold for the ‘autonomous change of direction’ condition (visualisation of a simulation can be found in the video supplement in Shirvani (2021)). Each run was set to start at  $t = -10$  min to allow the floodwater to propagate during 10 min so that the evacuation process starts at  $t = 0$  min. Outputs averaged from each series of simulation included spatial and temporal information, at each time step, about the pedestrian agents as they evacuate ( $t > 0$  min). The averaged outputs include the position, HR-related flood risk state, stability state (with a toppling-only condition, toppling-and-sliding condition and sliding-only condition), and the choice for the destination selected by the pedestrian agents during the evacuation process. Considering the stochastic uncertainties associated with the motion of the pedestrian agents, the plausibility of the averaged outputs from the 20 runs was evaluated. The evaluation was based on the *MOE*, using Eq. (3), for 99.9 % confidence level only, informed by the results of the analysis in Sec. 3.2. Table 6 shows the maximum *MOEs* found for the number of pedestrians predicted to be in the considered HR-related flood risk and the stability states, obtained from the 20 runs using each of the 20 %, 30 % and 40 % threshold, respectively. It can be seen that the maximum *MOE* increases as the risk perception level decreases, suggesting a notable increase in the uncertainty after the incorporation of the risk perception component into the modelling of pedestrian behaviours.

**Table 6:** Maximum margin of error (*MOE*) for the average number of pedestrian agents with different HR-related flood risk or stability states that are extracted from the recorded outputs throughout the simulations for each 20 %, 30 % and 40 % threshold. Different ranges of the evaluated maximum *MOE* are highlighted with different colour shades: green, orange and red to indicate  $MOE \leq \pm 5$ ,  $6 \leq MOE \leq 9$  and  $MOE \geq 10$ , respectively.

HR-related flood risk and stability states	Maximum <i>MOE</i>		
	20 % threshold	30 % threshold	40 % threshold
HR < 0.75	$\pm 16$	$\pm 16$	$\pm 19$
0.75 < HR < 1.5	$\pm 2$	$\pm 8$	$\pm 15$
HR > 1.5	$\pm 0$	$\pm 1$	$\pm 2$
Toppling-only	$\pm 2$	$\pm 5$	$\pm 13$
Toppling-and-sliding	$\pm 1$	$\pm 4$	$\pm 7$

Next, the averaged outputs are analysed for each of the 20 %, 30 % and 40 % thresholds, considering the popularity of the destination selected by the pedestrian agents (among south, east and north) together with their HR-related flood risk and stability states.

### 4.3 Analysis of the results

Figure 12 shows the trends in total number of evacuating pedestrians in the walkable area, plotted according to the pedestrians' choices among the south, east and north destinations, obtained from simulations with the 20 %, 30 % and 40 % threshold. All the simulated trends show a decrease in the total number of pedestrians after 25 min of flooding. This suggests that 25 min would be required for the 4,080 pedestrians to vacate the stadium, and that the choice for the threshold does not have any effect on the collective evacuation time.

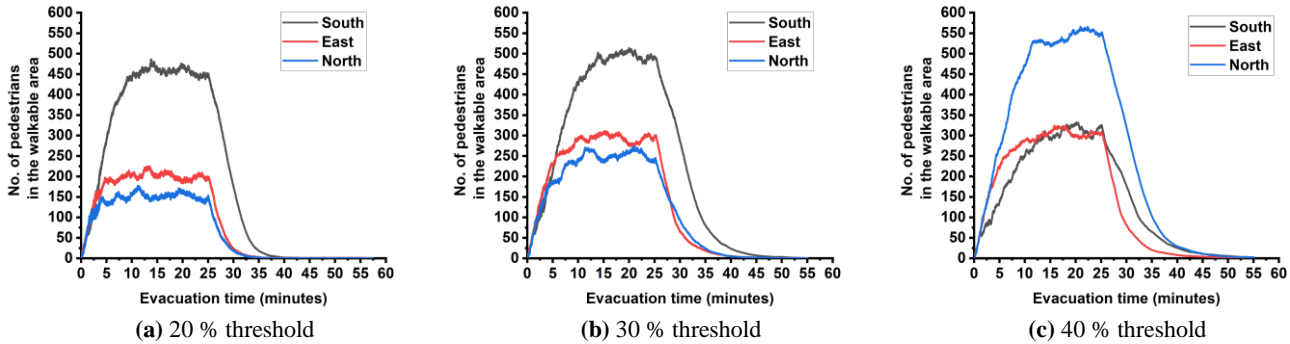
The simulated trends obtained with the 20 % threshold are shown in Fig. 12a, suggesting that most of the pedestrians evacuated the walkable area within almost 40 min. The majority of the evacuating pedestrians start favouring the south destination after 2.5 min, indicating that after this time pedestrians encounter floodwater depth beyond 20 % of their body height, which seems to be extending over the eastern and northern branches. After 2.5 min, the south destination remained the most popular destination, selected by more than 55 % of the pedestrians; whereas, the east and north destinations were less popular, selected by 25 % and 20 % of the pedestrians, respectively.

With the simulated trends obtained with the 30 % threshold (Fig. 12b), a longer evacuation time is predicted for the majority of the evacuating pedestrians. Now it takes about 52 min for most of the pedestrians to leave the walkable area and the popularity of the east and north destinations increased, with slightly more evacuating pedestrians preferring them, about 27 % and 23 %, respectively. This suggests that 5 % more of the pedestrians considered changing their destination to the north where the floodwater depth can only reach up to their knee height. Still, as with the 20 % threshold, the south destination was the most popular and started to be favoured after 5 min by 50 % of the pedestrians.

With the simulated trends obtained with the 40 % threshold (Fig. 12c), a significant change in the favoured destination is observed alongside a relatively more prolonged evacuation time. Now, it takes about 57 min for most of the pedestrians to evacuate the walkable area and the popularity of the south destination decreased significantly, compared to the predicted trends obtained with the lower thresholds. Here, the south destination was only picked up by 25 % of the pedestrians and the north destination was preferred instead (by around 50 % of the pedestrians) since the beginning of the evacuation. As for the east destination, it remained equally popular as with the trends obtained with the lower thresholds, and was selected by around 25 % of the evacuating pedestrians.

The simulated trends in Fig. 12 imply that the south destination would be preferred by people who are less likely to enter floodwater with a depth beyond their knee height, and that the north destination would be preferred by those willing to enter the deeper floodwater. The results also suggest longer evacuation times when people are willing to enter the floodwater at a depth beyond their knee height.

659



660

**Figure 12:** Total number of evacuating pedestrians in the walkable area plotted according to their destination choices for the south, east and north during the evacuation time: (a) 20 % threshold, (b) 30 % threshold and (c) 40 % threshold.

The trends for HR-related flood risk states and stability states averaged from simulations for each of the 20 %, 30 % and 40 % threshold are shown in Fig. 13. Fig. 13-left includes the HR-related flood risk states as well as the total number of evacuating pedestrians in the walkable area. As the threshold increases, the total number of pedestrians in the walkable area is seen to increase, leading to prolonged evacuation times. This observation is aligned with the trends in Fig. 12, suggesting that the evacuation process would be delayed as more evacuating pedestrians enter the deeper floodwater where their moving speed reduces. The number of pedestrians in dry zones remains constant, despite the choice for the threshold. This may be expected as these pedestrians represent those who initially decided to go to the south destination (one third of the pedestrians) and did not, therefore, find a need to alter their destination during the process given the dominance of dry areas over the southern branch (see Fig. 10a). For the three thresholds, the majority of the evacuating pedestrians were found to keep a low flood risk state ( $HR < 0.75$ ). Up to around 70 and 240 evacuating pedestrians reached a medium flood risk state ( $0.75 < HR < 1.5$ ) with the 30 % and 40 % thresholds, respectively, and no pedestrians were predicted to have the latter flood risk state with the 20 %

threshold. Up to only 5 pedestrians were detected at a high risk flood state ( $HR > 1.5$ ), namely from those who entered the floodwater at a depth beyond 40 % of their body height.

The number of evacuating pedestrians that could have a stability state with a toppling-only or toppling-and-sliding conditions are shown in Fig. 13-right. For the 20 % threshold, very few pedestrians were found to have these stability states, up to only 3 in number. Findings in Shirvani et al. (2020) suggest that these could be pedestrians with a low flood risk state ( $HR < 0.75$ ) with a toppling-only condition or with a medium flood risk state ( $0.75 < HR < 1.5$ ) with a toppling-and-sliding condition. The number of pedestrians with these stability states increased with the threshold of 30 %, which is expected given the increased number of pedestrians under low-to-medium flood risk states evacuating over a longer period. Up to 40 and 20 more pedestrians were found in toppling-only and toppling-and-sliding conditions, respectively. With the 40 % threshold, 25 more pedestrians were found to be in a toppling-and-sliding condition, and up to 100 more were found to be in a toppling-only condition. The significant increase in the number of pedestrians with a toppling-only condition is expected with the 40 % threshold, for which more pedestrians would be entering the floodwater where its depth is beyond their knee height.

The analysis of the HR-related flood risk and stability states suggests that the majority of people evacuating the stadium would take an evacuation route that is either dry or keeps them under a low flood risk state ( $HR < 0.75$ ) with a toppling-only condition during the evacuation. Less people would be entering deeper floodwaters and, when they do, they are expected to be in a medium flood risk state ( $0.75 < HR < 1.5$ ) where they can have a toppling-and-sliding condition.

690

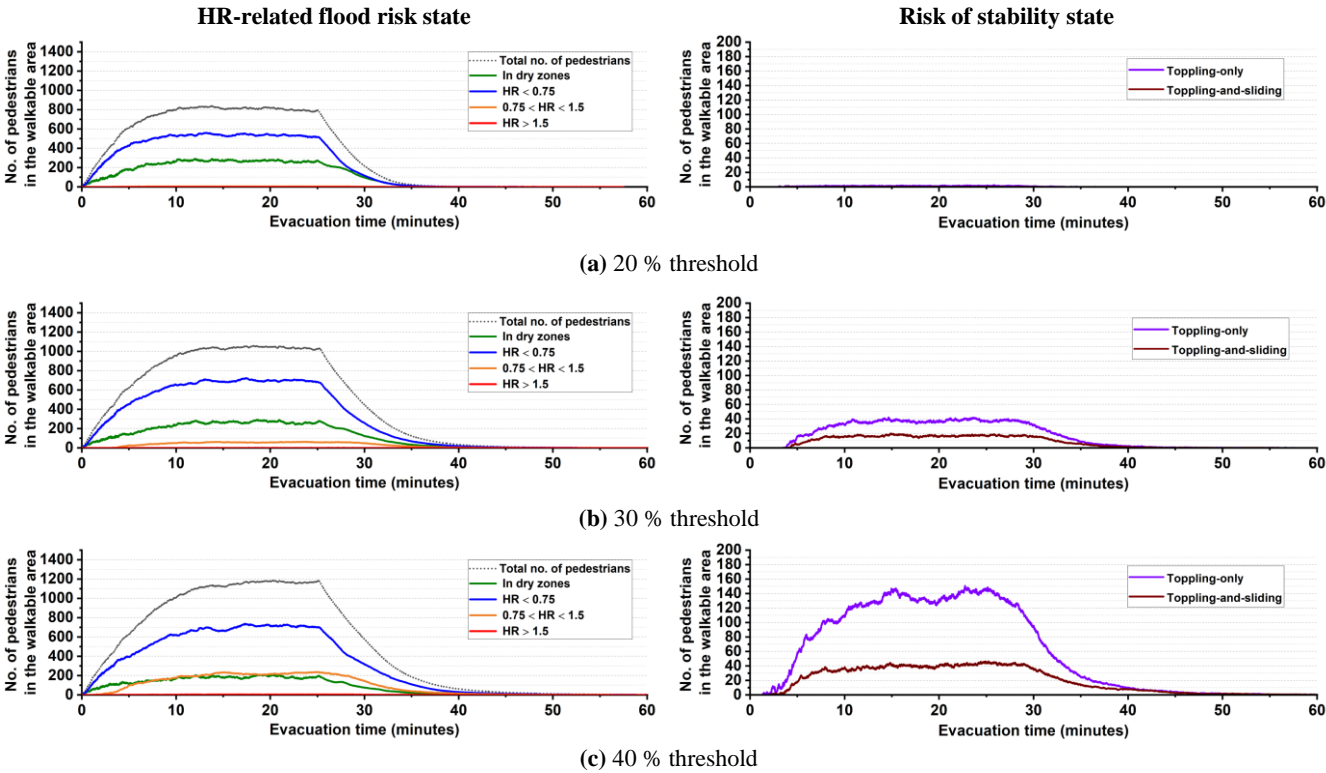


**Figure 13:** Total number of evacuating pedestrians in the walkable area plotted according to their HR-related flood risk state (left panel) and stability state when they were immobilised in floodwater (right panel) during the evacuation time: (a) 20 % threshold, (b) 30 % threshold and (c) 40 % threshold.

Figure 14 shows the 2D spatial distribution of the evacuating pedestrians over the HR flood map at 25 min when pedestrian presence in the walkable area is at its highest as soon as everyone vacates the stadium. The pedestrians are represented by dots with different colours representing their stability state based on the predictions made with the 20 %, 30 % and 40 % thresholds. The evacuation patterns in Figure 14, though retrieve the observations made before (through Fig. 12 and Fig. 13) demonstrate the simulator's further ability to inform on the potential locations where the evacuating pedestrians are expected to be immobilised by the floodwater. With the 20 % threshold (Fig. 14a), most of the pedestrians remained mobile in the floodwater (stable condition) and preferred the south destination where low flood HR dominates. From the remaining pedestrians, who preferred the east or north destinations, a handful were at risk of immobilisation (toppling-only or toppling-and-sliding conditions). These stability states are observed to occur particularly within northern and eastern branches where the flood HR varied from the upper low range to the medium range. The spatial distributions predicted with the 30 % threshold (Fig. 14b) also suggest a preference for the south destination by most of the pedestrians, and that many more pedestrians would be expected to be immobilised by the floodwater within the eastern and northern branches. There, at least a dozen would have a stability state with a toppling-and-sliding condition caused by the relatively higher number of pedestrians who kept moving to the north and east destinations. With the 40 % threshold (Fig. 14c), most of the pedestrians were still found to remain mobile in floodwater (stable condition) despite the fact that the (riskiest) north destination was the dominant choice. However, the spatial distributions predicted with this threshold point to a major increase in the number of immobilised pedestrians within the aforementioned vicinities.

The analysis in Fig. 14 suggests that people who avoid entering a floodwater depth beyond their knee height are most likely to select the south destination, where their condition remains stable to keep evacuating with minimum risk of immobilisation. Those with a tendency to enter deeper floodwaters would go to the east or north destinations, towards which the majority would still be able to evacuate, but at a slower pace delayed by the risk of facing immobilisation as they move forward to their selected destination. Overall, the predictions produced by the simulator (Fig. 12 to Fig. 14) seem useful in planning evacuation in outdoor spaces where the behaviour of pedestrians could be influenced by their autonomous decision making on the safest destination driven by their personal risk perception of the local floodwater and body height.

● Stable condition    ● Toppling-only condition    ● Toppling-and-sliding condition

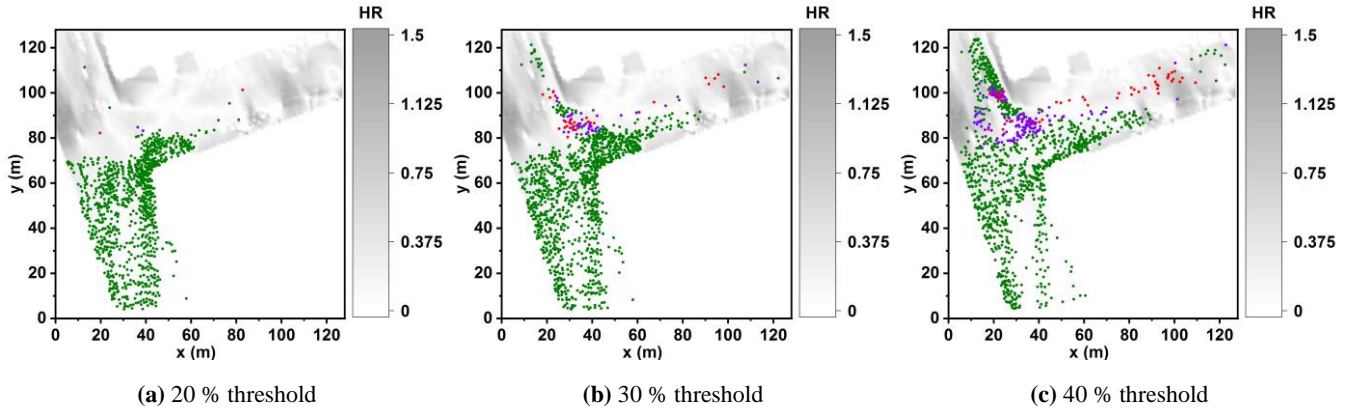


**Figure 14:** The spatial distribution of pedestrians over the walkable area under the predicted stability states (coloured dots) along with the HR flood map (grey shade) at simulation time  $t = 22$  min, when the number of pedestrians over the walkable area is at highest after all of them had vacated the stadium: (a) 20 % threshold, (b) 30 % threshold and (c) 40 % threshold.

## 5 Summary, discussions and limitations

The flood-pedestrian simulator was augmented to incorporate an enhanced level of heterogeneity in the pedestrian agent characterisation and realistic in-model rules governing their response to the floodwater. Pedestrians can now be characterised by age, gender and body mass attributes based on real-world datasets. The present simulator was also supported by a set of empirically based age- and gender-related moving speeds driving the motion of pedestrian agents around and inside the floodwater, and with a maximum excitement condition to accelerate the walking speed of pedestrian agents around the floodwater. The moving speed could also be intertwined with a two-way interaction condition to model the influence of pedestrian congestion on flowing floodwater, and vice versa. A new autonomous change of direction condition was proposed to model the way-finding decisions of pedestrian agents based on their individual perception of the flood risk in relation to the local changes in floodwater dynamics or the choice of others. The added features have enabled applying the simulator for outdoor spaces including multiple potential destinations for the pedestrians to detect during a flood evacuation.

The relevance of the added features were evaluated for a test case of a flood-induced evacuation in a shopping centre, which consists of an indoor space and was previously investigated for a basic version of the simulator with simpler pedestrian agent characterisation and behavioural rules. The evaluation procedure was based on systematically activating any of the added walking or running moving speeds with or without the two-way interaction condition in the simulator, and then analysing the changes induced in the simulation outcomes with reference to the baseline results. The analysis contrasted temporal and spatial changes in the number of pedestrians in relation to their HR-related flood risk and stability states, indicating major differences to the baseline results. The differences in the predicted number of pedestrians seems to vary considerably, up to hundreds, depending on the density of the crowd as the flood risk becomes low-to-medium. Also, the analysis suggests longer evacuation

741 times with the walking condition but using the running condition has led to the close evacuation times compared to baseline  
742 results.

743 The utility of the simulator, with the new autonomous change of direction condition, was then demonstrated over a  
744 real-world case study of evacuation of spectators from Sheffield's Hillsborough football stadium into a T-junction outdoor  
745 space leading to three ends towards the south, east and north destinations. The simulator was set up to replicate historical  
746 extents and depths of the floodwater that would inundate this study site. The autonomous change of direction condition was  
747 applied based on three thresholds of a floodwater depth to body height: 20% threshold, 30% threshold and 40% threshold,  
748 representative of a high, medium and low level of people's risk perception, respectively. The simulation outputs suggest that  
749 when people exhibit high to medium risk perception by avoiding zones with floodwater depth beyond their knee height, the  
750 majority change direction to go to the south destination that has the highest portion of dry zones. Whereas, when people exhibit  
751 a low risk perception and enter floodwaters higher than their knee height, the majority would take the shallowest pathway  
752 leading to the north destination. As the risk perception level decreased, the simulation output showed an increase in the number  
753 of people in a medium risk state with an immobilised condition and longer evacuation time. The investigations over the real-  
754 world case study demonstrates that the flood-pedestrian simulator can be used to analyse the dynamics of people's responses  
755 in and around the floodwater as part of the flood risk analysis; thus, it is a useful tool for planning evacuation of crowds to  
756 flood emergencies in small and potentially congested urban areas.

757 However, the flood-pedestrian simulator has a number of considerations and limitations that are worth mentioning.  
758 Firstly, the simulator requires the accessibility to a Graphical Processing Unit (GPU) card and the generation of input files  
759 requires special .xml translation specific to FLAMEGPU and using the FGPUGridNavPlanEditor toolkit, which is also made  
760 available online at: <https://github.com/RSE-Sheffield/FGPUGridNavPlanEditor>. Secondly, the simulator can provide a live  
761 visualisation showing hydrodynamic and pedestrian information changing in real time, when run on windows using the console  
762 mode (Shirvani, 2021). Thirdly, in terms of pedestrian characteristics, the simulator does not incorporate the uncertainties  
763 associated with social and psychological characteristics of people, e.g. flood tourism, as well as their floating and sinking  
764 conditions. Lastly, but not least, the assumptions and thresholds used to implement the two-way interaction condition and the  
765 autonomous change of direction condition are both lacking any existing empirical evidence base supported by dedicated  
766 laboratory experiments.

## 767 Code availability

768 The flood-pedestrian simulator is accessible from Zenodo open-access repository at <https://doi.org/10.5281/zenodo.4564288>,  
769 with a link to the GitHub source codes of the latest release, including a detailed 'run guide' and input files to enable the users  
770 to run the flooded shopping centre and the Hillsborough stadium evacuation test cases on their own machine. The previous  
771 version of the simulator is also available on DAFNI, available at: <https://dafni.ac.uk/project/flood-people-simulator/>, where it  
772 can be run from a user-friendly graphical interface and supported by a run guide.

773 **Data availability**

774 Outputs of the simulations are available in the Zenodo open-access repository at <https://doi.org/10.5281/zenodo.4576906>.

775 **Video supplement**

776 Demo videos of the test cases are available online in the TIB AV-Portal at <https://doi.org/10.5446/51547>.

777 **Author contribution**

778 MS contributed to developing the simulator, design of the test cases, running simulations, obtaining outputs and figure  
779 preparation. GK proposed the research approach and supervised the development, testing, scenario configurations and analysis  
780 of the outputs, and obtained the research grant. MS and GK prepared the manuscript. All authors read and approved the final  
781 paper.

782 **Competing interests**

783 The authors declare that they have no conflict of interest.

784 **Acknowledgements**

785 This work is part of the SEAMLESS-WAVE project (SoftwarE infrAstructure forMulti-purpose fLood modElling at variouS  
786 scaleS based on WAVElets), which is funded by the UK Engineering and Physical Sciences Research Council (EPSRC) grant  
787 EP/R007349/1. For information about the SEAMLESS-WAVE project visit <https://www.seamlesswave.com>. The authors wish  
788 to thank Paul Richmond and the Research Software Engineering (<https://rse.shef.ac.uk/>) group for providing technical support  
789 during the implementation of the flood-pedestrian simulator on FLAMEGPU.

790 **References**

791 Abebe, Y.A., Ghorbani, A., Nikolic, I., Manojlovic, N., Gruhn, A. and Vojinovic, Z.: The role of household adaptation  
792 measures in reducing vulnerability to flooding: a coupled agent-based and flood modelling approach, Hydrol. Earth Syst. Sci.,  
793 24, 5329-5354, <https://doi.org/10.5194/hess-24-5329-2020>, 2020.

794

795 Aboelata, M. and Bowles, D.S.: LIFESim: A tool for estimating and reducing life-loss resulting from dam and levee failures,  
796 in: Proceedings of the Association of State Dam Safety Officials “Dam Safety 2008” Conference, Indian Wells, California, 7–  
797 11 September, 533-574, <http://citeseerx.ist.psu.edu/viewdoc/summary?doi=10.1.1.155.2659>, 2008.

798

799 Aerts, J.C., Botzen, W.J., Clarke, K.C., Cutter, S.L., Hall, J.W., Merz, B., Michel-Kerjan, E., Mysiak, J., Surminski, S. and  
800 Kunreuther, H.: Integrating human behaviour dynamics into flood disaster risk assessment, *Nature Climate Change*, 8, 193-  
801 199, <https://doi.org/10.1038/s41558-018-0085-1>, 2018.

802

803 Aerts, J.C.: Integrating agent-based approaches with flood risk models: a review and perspective, *Water Security*, 11, 1-9,  
804 <https://doi.org/10.1016/j.wasec.2020.100076>, 2020.

805

806 Alonso Vicario S., Mazzoleni M., Bhamidipati S., Gharesifard M., Ridolfi E., Pandolfo C. and Alfonso L.: Unravelling the  
807 influence of human behaviour on reducing casualties during flood evacuation, *Hydrological Sciences Journal*, 65, 2359-2375,  
808 <https://doi.org/10.1080/02626667.2020.1810254>, 2020.

809

810 An, L., Grimm, V. and Turner II, B.L.: Meeting grand challenges in agent-based models, *Journal of Artificial Societies and*  
811 *Social Simulation*, 23, 13, <https://doi.org/10.18564/jasss.4012>, 2020.

812

813 Arrighi, C., Oumeraci, H. and Castelli, F.: Hydrodynamics of pedestrians' instability in floodwaters, *Hydrol. Earth Syst. Sci.*,  
814 21, 515-531, <https://doi.org/10.5194/hess-21-515-2017>, 2017.

815

816 Becker, J.S., Taylor, H.L., Doody, B.J., Wright, K.C., Gruntfest, E. and Webber, D.: A review of people’s behavior in and  
817 around floodwater, *Weather, Climate, and Society*, 7, 321-332, <https://doi.org/10.1175/WCAS-D-14-00030.1>, 2015.

818

819 Bernardini, G. and Quagliarini, E.: How to account for the human motion to improve flood risk assessment in urban areas,  
820 *Water*, 12, 1316, <https://doi.org/10.3390/w12051316>, 2020.

821

822 Bernardini, G., Postacchini, M., Quagliarini, E., Brocchini, M., Cianca, C. and D’Orazio, M.: A preliminary combined  
823 simulation tool for the risk assessment of pedestrians’ flood-induced evacuation, *Environmental Modelling and Software*, 96,  
824 14-29, <https://doi.org/10.1016/j.envsoft.2017.06.007>, 2017.

825

826 Bernardini, G., Quagliarini, E., D’Orazio, M. and Brocchini, M.: Towards the simulation of flood evacuation in urban  
827 scenarios: experiments to estimate human motion speed in floodwaters, *Safety Science*, 123, 104563,  
828 <https://doi.org/10.1016/j.ssci.2019.104563>, 2020.

829

830 Bernardini, G., Romano, G., Soldini, L. and Quagliarini, E.: How urban layout and pedestrian evacuation behaviours can  
831 influence flood risk assessment in riverine historic built environments, *Sustainable Cities and Society*, 70, 102876,  
832 <https://doi.org/10.1016/j.scs.2021.102876>, 2021.

833

834 Bert, F.E., Rovere, S.L., Macal, C.M., North, M.J. and Podestá, G.P.: Lessons from a comprehensive validation of an agent  
835 based-model: the experience of the pampas model of argentinean agricultural systems, *Ecological Modelling*, 273, 284-298,  
836 <https://doi.org/10.1016/j.ecolmodel.2013.11.024>, 2014.

837

838 Bohannon, R.W. and Andrews, A.W.: Normal walking speed: a descriptive meta-analysis, *Physiotherapy*, 97, 182-189,  
839 <https://doi.org/10.1016/j.physio.2010.12.004>, 2011.

840

841 Bring on the sub: Sheffield Wednesday's pitch submerged by flood water: Daily Mail Online (last access: 14 June 2021),  
842 [https://www.dailymail.co.uk/sport/football/article-464478/Bring-sub-Sheffield-Wednesdays-pitch-submerged-flood-](https://www.dailymail.co.uk/sport/football/article-464478/Bring-sub-Sheffield-Wednesdays-pitch-submerged-flood-water.html)  
843 [water.html](https://www.dailymail.co.uk/sport/football/article-464478/Bring-sub-Sheffield-Wednesdays-pitch-submerged-flood-water.html), 26 June 2007.

844

845 Chanson, H., Brown, R. and McIntosh, D.: Human body stability in floodwaters: the 2011 flood in Brisbane CBD, in:  
846 Proceedings of the 5th IAHR International Symposium on Hydraulic Structures, University of Queensland, Brisbane,  
847 Australia, 25-27 June 2014, 1-9, <https://doi.org/10.14264/uql.2014.48>, 2014.

848

849 Costabile, P., Costanzo, C., De Lorenzo, G. and Macchione, F.: Is local flood hazard assessment in urban areas significantly  
850 influenced by the physical complexity of the hydrodynamic inundation model?, *Journal of Hydrology*, 580, 124231,  
851 <https://doi.org/10.1016/j.jhydrol.2019.124231>, 2020.

852

853 Dawson, R.J., Peppe, R. and Wang, M.: An agent-based model for risk-based flood incident management, *Natural Hazards*,  
854 59, 167-189, <https://doi.org/10.1007/s11069-011-9745-4>, 2011.

855

856 Dias, C., Abd Rahman, N. and Zaiter, A.: Evacuation under flooded conditions: Experimental investigation of the influence of  
857 water depth on walking behaviors. *International Journal of Disaster Risk Reduction*, 58, 102192,  
858 <https://doi.org/10.1016/j.ijdr.2021.102192>, 2021.

859

860 Disabled World: Adult Body Mass Index (BMI) Calculator and Table, Disabled World, [https://www.disabled-](https://www.disabled-world.com/calculators-charts/bmi.php)  
861 [world.com/calculators-charts/bmi.php](https://www.disabled-world.com/calculators-charts/bmi.php), 2017.

862

863 Dobbs, R.J., Charlett, A., Bowes, S.G., O'Neill, C.J.A., Weller, C., Hughes, J. and Dobbs, S.M.: Is this walk normal?, Age and  
864 Ageing, 22, 27-30, <https://doi.org/10.1093/ageing/22.1.27>, 1993.

865

866 Engineering ToolBox: Room Area per Person, available at: [https://www.engineeringtoolbox.com/number-persons-buildings-](https://www.engineeringtoolbox.com/number-persons-buildings-d_118.html)  
867 [d\\_118.html](https://www.engineeringtoolbox.com/number-persons-buildings-d_118.html) (last access: 15 January 2021), 2003.

868

869 Environment Agency: Review of 2007 summer floods, Environment Agency, Almondsbury, Bristol, United Kingdom,  
870 available at:  
871 [https://assets.publishing.service.gov.uk/government/uploads/system/uploads/attachment\\_data/file/292924/geho1107bnmi-e-](https://assets.publishing.service.gov.uk/government/uploads/system/uploads/attachment_data/file/292924/geho1107bnmi-e-e.pdf)  
872 [e.pdf](https://assets.publishing.service.gov.uk/government/uploads/system/uploads/attachment_data/file/292924/geho1107bnmi-e-e.pdf) (last access: 22 January 2021), 2007.

873

874 Fielding, J., Burningham, K., Thrush, D. and Catt, R.: Public response to flood warning: R&D Technical Report SC020116,  
875 Department for the Environment, Food and Rural Affairs (DEFRA), UK, available at  
876 [https://assets.publishing.service.gov.uk/media/602d3a81d3bf7f721c13a3ba/Public\\_response\\_to\\_flood\\_warning\\_technical\\_re](https://assets.publishing.service.gov.uk/media/602d3a81d3bf7f721c13a3ba/Public_response_to_flood_warning_technical_report.pdf)  
877 [port.pdf](https://assets.publishing.service.gov.uk/media/602d3a81d3bf7f721c13a3ba/Public_response_to_flood_warning_technical_report.pdf) (last accessed 21 May 2021), 2007.

878

879 Flood and coastal erosion risk management policy statement, Department for Environment, Food and Rural Affairs, available  
880 at: <https://www.gov.uk/government/publications/flood-and-coastal-erosion-risk-management-policy-statement> (last access:  
881 03 March 2021), 14 July 2020.

882

883

884 Football Webpages: Sheffield Wednesday, <https://www.footballwebpages.co.uk/sheffield-wednesday>, last access: 03 March  
885 2021.

886

887 Hamilton, K., Demant, D., Peden, A.E. and Hagger, M.S.: A systematic review of human behaviour in and around floodwater,  
888 International Journal of Disaster Risk Reduction, 47, 101561, <https://doi.org/10.1016/j.ijdr.2020.101561>, 2020.

889

890 Hazra, A.: Using the confidence interval confidently, J. Thorac. Dis., 9, 4125–4130,  
891 <https://dx.doi.org/10.21037/2Fjtd.2017.09.14>, 2017.

892

893 Helbing, D. and Molnar, P.: Social force model for pedestrian dynamics, Phys. Rev. E, 51, 4282,  
894 <https://doi.org/10.1103/PhysRevE.51.4282>, 1995.

895

896 Ishigaki, T., Kawanaka, R., Onishi, Y., Shimada, H., Toda, K. and Baba, Y.: Assessment of safety on evacuating route during  
897 underground flooding, in: *Advances in Water Resources and Hydraulic Engineering: Proceedings of 16th IAHR-APD*  
898 *Congress and 3rd Symposium of IAHR-ISHS*, Springer, Berlin, Heidelberg, 141-146, [https://doi.org/10.1007/978-3-540-](https://doi.org/10.1007/978-3-540-89465-0)  
899 [89465-0](https://doi.org/10.1007/978-3-540-89465-0), 2009.

900

901 Jiang, Y., Chen, B., Li, X. and Ding, Z.: Dynamic navigation field in the social force model for pedestrian evacuation, *Applied*  
902 *Mathematical Modelling*, 80, 815-826, <https://doi.org/10.1016/j.apm.2019.10.016>, 2020.

903

904 Karmakharm, T., Richmond, P. and Romano, D.M.: Agent-based large scale simulation of pedestrians with adaptive realistic  
905 navigation vector fields, *Theory and Practice of Computer Graphics*, 10, 67-74,  
906 <http://dx.doi.org/10.2312/LocalChapterEvents/TPCG/TPCG10/067-074>, 2010.

907

908 Kvočka, D., Falconer, R.A. and Bray, M.: Flood hazard assessment for extreme flood events, *Natural Hazards*, 84, 1569-1599,  
909 <https://doi.org/10.1007/s11069-016-2501-z>, 2016.

910

911 Lange, D.: Share of people who have attended at least two live sports events in the last year in England from May 2018 to May  
912 2020 by age, available at: <https://www.statista.com/statistics/783771/live-sports-events-spectators-england-by-by-age/> (last  
913 access 03 March 2021), 2020.

914

915 Lee, H.K., Hong, W.H. and Lee, Y.H.: Experimental study on the influence of water depth on the evacuation speed of elderly  
916 people in flood conditions, *International Journal of Disaster Risk Reduction*, 39, 101198,  
917 <https://doi.org/10.1016/j.ijdr.2019.101198>, 2019.

918

919 Li, M., Wei, Y. and Xu, Y.: A route navigation algorithm for pedestrian simulation based on grid potential field, *Advances in*  
920 *Mechanical Engineering*, 11, 1–13, <https://doi.org/10.1177%2F1687814019897831>, 2019.

921

922 Lin, J., Zhu, R., Li, N. and Becerik-Gerber, B.: Do people follow the crowd in building emergency evacuation? A cross-cultural  
923 immersive virtual reality-based study, *Advanced Engineering Informatics*, 43, 101040,  
924 <https://doi.org/10.1016/j.aei.2020.101040>, 2020.

925

926 Liu, X. and Lim, S.: Integration of spatial analysis and an agent-based model into evacuation management for shelter  
927 assignment and routing, *Journal of spatial science*, 61, 283-298, <https://doi.org/10.1080/14498596.2016.1147393>, 2016.

928

929 Lumbroso, D. and Davison, M.: Use of an agent-based model and Monte Carlo analysis to estimate the effectiveness of  
930 emergency management interventions to reduce loss of life during extreme floods, *Journal of Flood Risk Management*, 11,  
931 S419-S433, <https://doi.org/10.1111/jfr3.12230>, 2018.

932

933 Lumbroso, D. and Di Mauro, M.: Recent developments in loss of life and evacuation modelling for flood event management  
934 in the UK, *WIT Transactions on Ecology and the Environment*, 118, 263-272, <https://doi.org/10.2495/FRIAR080251>, 2008.

935

936 Lumbroso, D., Davison, M., Body, R., and Petkovšek, G.: Modelling the Brumadinho tailings dam failure, the subsequent loss  
937 of life and how it could have been reduced, *Nat. Hazards Earth Syst. Sci.*, 21, 21–37, [https://doi.org/10.5194/nhess-21-21-](https://doi.org/10.5194/nhess-21-21-2021)  
938 [2021](https://doi.org/10.5194/nhess-21-21-2021), 2021.

939

940 Lumbroso, D.M., Sakamoto, D., Johnstone, W.M., Tagg, A.F. and Lence, B.J.: Development of a life safety model to estimate  
941 the risk posed to people by dam failures and floods, *Dams and Reservoirs*, 21, 31-43,  
942 <https://doi.org/10.1680/dare.2011.21.1.31>, 2011.

943

944 Mas, E., Koshimura, S., Imamura, F., Suppasri, A., Muhari, A. and Adriano, B.: Recent advances in agent-based tsunami  
945 evacuation simulations: case studies in Indonesia, Thailand, Japan and Peru, *Pure and Applied Geophysics*, 172, 3409-3424,  
946 <https://doi.org/10.1007/s00024-015-1105-y>, 2015.

947

948 Matsuo, K., Natainia, L. and Yamada, F.: Flood and evacuation simulations for urban flooding, 5th International Conference  
949 on Flood Management, Tokyo, Japan, 27-29 September 2011, 391-398, 2011.

950

951 McClymont, K., Morrison, D., Beevers, L. and Carmen, E.: Flood resilience: a systematic review, *Journal of Environmental*  
952 *Planning and Management*, 63, 1151-1176, <https://doi.org/10.1080/09640568.2019.1641474>, 2020.

953

954 Milanesi, L., Pilotti, M. and Ranzi, R.: A conceptual model of people's vulnerability to floods, *Water Resour. Res.*, 51, 182-  
955 197, <https://doi.org/10.1002/2014WR016172>, 2015.

956

957 Minegishi, Y. and Takeichi, N.: Design guidelines for crowd evacuation in a stadium for controlling evacuee accumulation  
958 and sequencing, *Japan Architectural Review*, 1, 471-485, <https://doi.org/10.1002/2475-8876.12042>, 2018.

959

960 Moftakhari, H.R., AghaKouchak, A., Sanders, B.F., Allaire, M. and Matthew, R.A.: What is nuisance flooding? Defining and  
961 monitoring an emerging challenge, *Water Resour. Res.*, 54, 4218-4227, <https://doi.org/10.1029/2018WR022828>, 2018.

962

963 Mohler, B.J., Thompson, W.B., Creem-Regehr, S.H., Pick, H.L. and Warren, W.H.: Visual flow influences gait transition  
 964 speed and preferred walking speed, *Experimental Brain Research*, 181, 221-228, <https://doi.org/10.1007/s00221-007-0917-0>,  
 965 2007.

966

967 Musolino, G., Ahmadian, R., Xia, J. and Falconer, R.A.: Mapping the danger to life in flash flood events adopting a mechanics  
 968 based methodology and planning evacuation routes, *Journal of Flood Risk Management*, 13, e12627,  
 969 <https://doi.org/10.1111/jfr3.12627>, 2020.

970

971 Netzel, L.M., Heldt, S., Engler, S. and Denecke, M.: The importance of public risk perception for the effective management  
 972 of pluvial floods in urban areas: a case study from Germany, *Journal of Flood Risk Management* [early view],  
 973 <https://doi.org/10.1111/jfr3.12688>, 2021.

974

975 Polhill, J.G., Sutherland, L.A. and Gotts, N.M.: Using qualitative evidence to enhance an agent-based modelling system for  
 976 studying land use change, *Journal of Artificial Societies and Social Simulation*, 13, 10, <https://doi.org/10.18564/jasss.1563>,  
 977 2010.

978

979 Prentice, A.M.: Body mass index standards for children: are useful for clinicians but not yet for epidemiologists, *Br. Med. J.*  
 980 (Clin. Res. Ed.), 317, 1401-1402, <https://dx.doi.org/10.1136%2Fbmj.317.7170.1401>, 1998.

981

982 Priest, S. J.: Why understanding behaviour matters for flood risk management?, *Journal of Flood Risk Management*, 14,  
 983 e12724, <https://doi.org/10.1111/jfr3.12724>, 2021.

984

985 Pugh, W.: Severe flooding near Hillsborough will not stop Sheffield Wednesday's game against Swansea being played  
 986 tomorrow despite homes nearby being evacuated, <https://www.thesun.co.uk/sport/football/10303677> (last access: 03 March  
 987 2021), 2019.

988

989 Ramsbottom, D., Wade, S., Bain, V., Hassan, M., Penning-Rowsell, E., Wilson, T., Fernandez, A., House, M. and Floyd, P.:  
 990 Flood risks to people methodology: Phase 2. R&D Technical Report FD2321/TR2, Department for the Environment, Food  
 991 and Rural Affairs (DEFRA), UK, available at  
 992 [http://sciencesearch.defra.gov.uk/Document.aspx?Document=FD2321\\_3436\\_TRP.pdf](http://sciencesearch.defra.gov.uk/Document.aspx?Document=FD2321_3436_TRP.pdf) (last access: 15 December 2020),  
 993 2006.

994

995 Rufat, S., Fekete, A., Armaş, I., Hartmann, T., Kuhlicke, C., Prior, T., Thaler, T. and Wisner, B.: Swimming alone? Why  
 996 linking flood risk perception and behavior requires more than “it's the individual, stupid”, *WIREs Water*, 7, e1462,  
 997 <https://doi.org/10.1002/wat2.1462>, 2020.

998

999 Shirvani, M, Kesserwani, G, Richmond, P.: Agent-based simulator of dynamic flood-people interactions, *Journal of Flood*  
 1000 *Risk Management*, 14, e12695, <https://doi.org/10.1111/jfr3.12695>, 2021.

1001

1002 Shirvani, M, Kesserwani, G.: Flood-pedestrian simulator, Zenodo [code], <https://doi.org/10.5281/zenodo.4564288>, 2021a.

1003

1004 Shirvani, M, Kesserwani, G.: Outputs of the flood-pedestrian simulator applied to the flooded shopping centre and  
 1005 Hillsborough Stadium test cases, Zenodo [data set], <https://doi.org/10.5281/zenodo.4576906>, 2021b.

1006

1007 Shirvani, M., Kesserwani, G. and Richmond, P.: Agent-based modelling of pedestrian responses during flood emergency:  
 1008 mobility behavioural rules and implications for flood risk analysis, *Journal of Hydroinformatics*, 22, 1078-1092,  
 1009 <https://doi.org/10.2166/hydro.2020.031>, 2020.

1010

1011 Shirvani, M.: Flood-pedestrian simulator video demos, TIB AV-Portal [video], <https://doi.org/10.5446/51547>, 2021.

1012

1013 Statista Research Department: Europe: distribution of football fans in 2016, by country and gender, available at:  
 1014 <https://www.statista.com/statistics/658959/europe-football-fans-by-country-and-gender/> (last access 03 March 2021), 2016.

1015

1016 Still, G.K.: Crowd Safety and Crowd Risk Analysis, Crowd Risk Analysis Ltd, available at:  
 1017 <https://www.gkstill.com/Support/crowd-density/CrowdDensity-1.html> (last access: 03 March 2021), 2019.

1018

1019 Teichtahl, A.J., Wluka, A.E., Strauss, B.J., Wang, Y., Berry, P., Davies-Tuck, M. and Cicuttini, F.M.: The associations between  
 1020 body and knee height measurements and knee joint structure in an asymptomatic cohort, *BMC Musculoskeletal Disorders*, 13,  
 1021 1-7, <https://doi.org/10.1186/1471-2474-13-19>, 2012.

1022

1023 **The Sheffield Guide by DeeJayOne: Sheffield Floods: SWFC, Hillsborough Stadium and River Don // Sheffield Guide, online**  
 1024 **video clip, YouTube (last access: 14 June 2021), <https://www.youtube.com/watch?v=dbkizUtNSqA>, 27 June 2007.**

1025

1026 Toor, A., Happer, A., Overgaard, R. and Johal, R.: Real world walking speeds of young pedestrians, *SAE International*, 110,  
 1027 1106-1114, <http://www.jstor.org/stable/44730963>, 2001.

1028

1029 UK population by ethnicity, Office for National Statistics [data set], available at: [https://www.ethnicity-facts-](https://www.ethnicity-facts-figures.service.gov.uk/uk-population-by-ethnicity)  
1030 [figures.service.gov.uk/uk-population-by-ethnicity](https://www.ethnicity-facts-figures.service.gov.uk/uk-population-by-ethnicity) (last access: 03 March 2021), 2018.  
1031  
1032 Willis, T., Wright, N. and Sleight, A.: Systematic analysis of uncertainty in 2D flood inundation models, *Environmental*  
1033 *Modelling and Software*, 122, 104520, <https://doi.org/10.1016/j.envsoft.2019.104520>, 2019.  
1034  
1035 Xia, J., Falconer, R.A., Wang, Y. and Xiao, X.: New criterion for the stability of a human body in floodwaters, *Journal of*  
1036 *Hydraulic Research*, 52, 93-104, <https://doi.org/10.1080/00221686.2013.875073>, 2014.  
1037  
1038 Zhu, X., Dai, Q., Han, D., Zhuo, L., Zhu, S., and Zhang, S.: Modelling the high-resolution dynamic exposure to flooding in a  
1039 city region, *Hydrol. Earth Syst. Sci.*, 23, 3353–3372, <https://doi.org/10.5194/hess-23-3353-2019>, 2019.  
1040  
1041 Zhuo, L. and Han, D.: Agent-based modelling and flood risk management: a compendious literature review, *Journal of*  
1042 *Hydrology*, 591, 125600, <https://doi.org/10.1016/j.jhydrol.2020.125600>, 2020.  
1043